Identification of a mechanism promoting mitochondrial sterol accumulation during myocardial ischemia–reperfusion: role of TSPO and STAR

Juliette Bréhat, Shirin Leick, Julien Musman, Jin Bo Su, Nicolas Eychenne, Frank Giton, Michael Rivard, Louis-Antoine Barel, Chiara Tropeano, Frederica Vitarelli, et al.

Identification of a mechanism promoting mitochondrial sterol accumulation during myocardial ischemia-reperfusion: role of TSPO and STAR.

Juliette Bréhat[1], Shirin Leick[1], Julien Musman[1], Jin Bo Su[1], Nicolas Eychenne[2], Frank Giton[3], Michael Rivard[4], Louis-Antoine Barel[4], Chiara Tropeano[5], Frederica Vitarelli[5], Claudio Caccia[6], Valerio Leoni[5], Bijan Ghaleh[1], Sandrine Pons[1] and Didier Morin[1,*]

[1]INSERM U955-IMRB, team Ghaleh, UPEC, Ecole Nationale Vétérinaire d'Alfort, Créteil, France.
[2]CHIV, Villeneuve-Saint-Georges, France
[3]Hôpital Henri Mondor, Pôle Biologie-Pathologie, IMRB U955, Créteil, France.
[4]UPEC, CNRS, ICMPE, UMR 7182, Thiais, France.
[5]Laboratory of Clinical Chemistry, Hospital Pio XI Desio, ASST-Brianza Department of Medicine and Surgery, University of Milano Bicocca, Monza, Italy
[6]Unit of Medical Genetics and Neurogenetics. Fondazione IRCCS – Istituto Neurologico Carlo Besta, Milano, Italy

Juliette Bréhat and Shirin Leick have contributed equally to this work.

*Corresponding author: Didier MORIN, PhD, INSERM U955, Team Ghaleh, Faculté de Santé, 8 rue du général Sarrail, 94000, Créteil, France, E-mail : didier.morin@inserm.fr.

List of abbreviations

CYP: cytochrome P450; GAPDH: glyceraldehyde 3-phosphate dehydrogenase; SOD2: superoxide dismutase 2 cytochrome; COX-IV; cytochrome C oxidase; TSPO: translocator protein; STAR: steroidogenic acute regulatory protein; mPTP: mitochondrial permeability transition pore; VDAC: voltage-dependent anion channel; ROS: reactive oxygen species; AUC: area under the curve; AOC: area over curve.

Abstract

Hypercholesterolemia is a major risk factor for coronary artery diseases and cardiac ischemic events. Cholesterol per se could also have negative effects on the myocardium, independently from hypercholesterolemia. Previously, we reported that myocardial ischemia-reperfusion induces a deleterious build-up of mitochondrial cholesterol and oxysterols, which is potentiated by hypercholesterolemia and prevented by translocator protein (TSPO) ligands. Here, we studied the mechanism by which sterols accumulate in cardiac mitochondria and promote mitochondrial dysfunction. We performed myocardial ischemia-reperfusion in rats to evaluate mitochondrial function, TSPO and steroidogenic acute regulatory protein (STAR) levels and the related mitochondrial concentrations of sterols. Rats were treated with the cholesterol synthesis inhibitor pravastatin or the TSPO ligand 4'-chlorodiazepam. We used *Tspo* deleted rats, which were phenotypically characterized. Inhibition of cholesterol synthesis reduced mitochondrial sterol accumulation and protected mitochondria during myocardial ischemia-reperfusion. We found that cardiac mitochondrial sterol accumulation is the consequence of enhanced influx of cholesterol and not of the inhibition of its mitochondrial metabolism during ischemia-reperfusion. Mitochondrial cholesterol accumulation at reperfusion was related to an increase in mitochondrial STAR but not to changes in TSPO levels. 4'-Chlorodiazepam inhibited this mechanism and prevented mitochondrial sterol accumulation and mitochondrial ischemia-reperfusion injury, underlying the close cooperation between STAR and TSPO. Conversely, *Tspo* deletion, which did not alter cardiac phenotype, abolished the effects of 4'-chlorodiazepam. This study reveals a novel mitochondrial interaction between TSPO and STAR to promote cholesterol and deleterious sterol mitochondrial accumulation during myocardial ischemia-reperfusion. This interaction regulates mitochondrial homeostasis and plays a key role during mitochondrial injury.

Keywords: myocardial ischemia-reperfusion; mitochondria; translocator protein; steroidogenic acute regulatory protein.

Introduction

Ischemic heart disease is a leading cause of morbidity and mortality worldwide with a constant increasing prevalence and development of novel cardioprotective strategies remains necessary [28,55]. Although numerous studies have shown their ability to confer cardioprotection in animal models, the translation of these promising results into clinical setting has been disappointing. The global lack of consideration of co-morbidities in preclinical studies is considered as one of the reasons for this large-scale failure [9,29,31].

Hypercholesterolemia is considered as a principal risk factor for coronary artery diseases. High circulating levels of cholesterol contribute to the formation of atheroma plaques and thus to the induction of ischemic pathologies. Thereby, patients with high hypercholesterolemia have an elevated risk of ischemic events [60] and lipid-lowering therapies are associated with delayed cardiovascular events and prolonged survival [43,54]. This elevated risk is attributed to the development of atherosclerosis as a result of hypercholesterolemia. However, during the last decades, several experimental and clinic observations have shown that hypercholesterolemia per se could also exerts direct negative effects on the myocardium, inducing alterations of the structure and the function of the cardiomyocytes [30,64]. It may interfere with cardioprotective mechanisms [1]. The molecular mechanisms by which hypercholesterolemia directly alters cardiac cells are ill known. Some data indicate that hypercholesterolemia induces oxidative stress [36,46], apoptosis [47] and favors opening of the mitochondrial permeability transition pore (mPTP) [36,41] which is a key event contributing to myocardial reperfusion injury [25].

The mitochondrial translocator protein (18 kDa; TSPO) is a high affinity cholesterol binding protein primarily located in the outer mitochondrial membrane and is expressed in a wide variety of species and ubiquitously distributed with a predominantly expression in steroid-synthesizing tissues [39]. TSPO is also abundant in kidney and heart. In steroidogenic tissues, TSPO seems to be part of a dynamic complex including outer mitochondrial membrane proteins such as the voltage-dependent anion channel (VDAC) and cytosolic proteins such as the steroidogenic acute regulatory protein (STAR) which is the principal mean pathway of cholesterol transport from lipid droplets to mitochondria [37,50]. STAR is synthesized as a 37-kDa protein, targeted to mitochondria, through its mitochondrial signal, where it is processed by proteases in the outer mitochondrial membrane to a mature 30-kDa form [2,3]. The role of TSPO in mPTP opening was largely discussed but its participation in mPTP formation was dismissed using a cardiac mouse *Tspo* gene deleted model [59]. However, a body of evidence suggests that TSPO plays a critical role in regulating physiological cardiac function and that TSPO ligands may represent interesting drugs to protect the heart during ischemia-reperfusion [39]. Indeed, several TSPO ligands such as SSR180575, 4'-chlorodiazepam or TRO40303 demonstrated cardioprotective effects by reducing infarct size in different animal models of myocardial infarction [32,45,58]. This effect was associated with a protection of mitochondrial function and a limitation of the increase in mitochondrial membrane permeability.

We previously demonstrated that the reperfusion of an ischemic myocardium causes a large increase in mitochondrial cholesterol content and a subsequent strong generation of auto-oxidized oxysterols resulting from the oxidation of cholesterol by reactive oxygen species (ROS). Oxysterols, whether formed endogenously or brought in certain foods, have major cytotoxic properties [65]. This mitochondrial accumulation of sterols at reperfusion was dramatically enhanced in hyper-cholesterolemic animals [41]. Interestingly, TSPO ligands

inhibited cholesterol and concomitant auto-oxidized oxysterol accumulation, limited the increase in mitochondrial membrane permeability and protected mitochondrial function both in normo- and hyper-cholesterolemic animals [41,45,51]. Although some genetic experiments questioned the involvement of TSPO in the mitochondrial transport of cholesterol [5,62], the inhibition of cholesterol and oxysterol accumulation could represent a promising approach to limit mitochondrial injury during myocardial ischemia-reperfusion and, thus, could participate to the cardioprotective effect of TSPO ligands.

Here, to verify this hypothesis, we examined whether the inhibition of cholesterol synthesis led to the inhibition of mitochondrial cholesterol and oxysterol accumulation and concomitantly protected mitochondrial functions during myocardial ischemia-reperfusion. Then, we investigated the mechanism by which cholesterol accumulates into mitochondria during myocardial reperfusion by determining whether this accumulation results from an increase in cholesterol influx and/or a decrease in cholesterol conversion. To do that: (1) we investigated the potential role of the proteins that convert cholesterol inside mitochondria, *i.e.*, the cytochromes P450 (CYP) 11A1 and 27A1; (2) we studied the role of the main proteins that have been described to participate in the transport of cholesterol into mitochondria of steroidogenic organs, *i.e*, TSPO and STAR. For this purpose, we used the TSPO ligand 4'-chlorodiazepam and TSPO global knock-out rats (*Tspo*$^{-/-}$).
Our data demonstrate that the inhibition of cholesterol synthesis protects mitochondria against ischemia-reperfusion injury and indicate that mitochondrial processing of STAR is required to transfer cholesterol into mitochondria during myocardial ischemia-reperfusion, a process that is modulated by TSPO.

Methods

Animals

Male Wistar and Sprague Dawley rats (≈ 300g) were used in this study. All animals were maintained under optimal environmental conditions (temperature 22-25°C and a constant cycle of 12-h light/dark) in the animal house of the faculty of Medicine of the University Paris-Est (approval number E94028028).
Male Wistar rats were purchased from Janvier (Le Genest-St-Isle, France). A couple of heterozygous global *Tspo* knock-out Sprague Dawley rats (*Tspo*$^{+/-}$) has been kindly provided by Pr Papadopoulos (University of Southern California, USA). These Sprague Dawley rats carried out a 89bp deletion in the *Tspo* gene resulting in the absence of protein expression [48]. These animals were crossed to generate of wild-type (*Tspo*$^{+/+}$) and homozygous *Tspo*

deleted (*Tspo*$^{-/-}$) rats. *Tspo*$^{+/+}$ and *Tspo*$^{-/-}$ rats are either littermates or generated from littermates to avoid generating high percentage of pups not needed from heterozygous breeding for ethical considerations. In addition, the animals were used after height generations of back-crossing. All rats used in this study were PCR genotyped using specific primers (Fig. 1a) and no TSPO immunoreactive protein was detected in myocardium (Fig. 1b) and cardiac mitochondria (Fig. 1c) of *Tspo*$^{-/-}$ rats. Cardiac morphology was similar between both genotypes and *Tspo*$^{-/-}$ rats did not display alterations in left ventricular function. This absence of cardiac phenotype variation persisted during aging (Online Fig. S1 and Online Fig. S2). *Tspo* deletion did not alter rat reproduction and morphology (Online Fig. S3a and S3b) although *Tspo*$^{-/-}$ rats tend to have a lower body weight (Online Fig. S3c). In the same way, we did not observe major differences concerning circulating steroidogenic hormones (Online Fig. S3d), basal glucose and lipid blood levels between both genotypes during aging (Online Fig. S4a) and both genotypes respond identically when subjected to metabolic tests, *i.e*., insulin and glucose tolerance tests (Online Fig. S4b and S4c).

In vivo coronary artery occlusion-reperfusion

Rats were subjected to 30 min of ischemia followed by 15 min of reperfusion. Rats were anesthetized with ketamine (100 mg/kg) and xylazine (10 mg/kg) given intraperitoneally. The depth of anesthesia was monitored using the tail pinching response and the pedal reflex. Once anesthetized, rats were placed on a warming pad to maintain body temperature at 37°C (Homeothermic Blanket Control Unit, Harvard Apparatus, Les Ulis, France). Then, the animals were intubated using an endotracheal tube and artificially ventilated with a rodent ventilator model VentElite (respiratory rate, 63/min; respiratory volume, 2.20 mL; Harvard Apparatus, Les Ulis, France) with a mixture of carbogen (95% O_2, 5% CO_2).

A left thoracotomy in the fourth intercostal space was performed, followed by pericardectomy, using a surgical microscope. A surgical needle with a 5–0 Prolene thread was passed around the left coronary artery, and the ends of the suture were passed through a polypropylene tube to form a snare. Tightening the snare induced coronary artery occlusion and its release initiated reperfusion for 15 min. This reperfusion duration was chosen because mPTP opening was shown to occur within the first minutes of reperfusion [24]. In parallel, sham animals were subjected to same surgical procedure but the coronary artery was not occluded.

4'-Chlorodiazepam (10 mg/kg) or its vehicle (dimethylsulfoxide) were administered intravenously through the jugular vein. This dose of 4'-chlorodiazepam was selected because it was shown to be cardioprotective in a previous study [45]. In the ischemia-reperfused group, 4'-chlorodiazepam were injected 10 min before reperfusion during a 5 min infusion. For the sham group, the drugs were administered 25 min before heart excision.

Pravastatin (10mg/kg) was given by gavage three days before surgery. We chose this dose and a short duration of treatment because the aim was to limit cholesterol metabolism to decrease cellular cholesterol available for mitochondria and not to induce hypocholesterolemia. The molecule was dissolved in the drinking water at a concentration of 10mg/mL and administered orally at 10mg/kg per day. Animals underwent surgical procedures 24 hours after the last administration.

At the end of 15 minutes of reperfusion, the heart was excised and the left ventricular area at risk of ischemia-reperfused rats or the left ventricle for sham rats were used to prepare mitochondria and cytosols. To delineate the area at risk, both the position of the suture used for the coronary artery occlusion and the change in coloration of the myocardium at the area at risk level during the occlusion were used. This allowed avoiding any contamination of the area at risk by a dye that could impair mitochondrial functions. The weight of the area at risk varied from 190-220 mg according to the experiments. The same area of the myocardium was excised from sham animals (myocardium not subjected to ischemia-reperfusion) to analyse mitochondrial functions.

To determine infarct size, the same ischemia-reperfusion procedure was applied but the chest was closed in layers and the pneumothorax was evacuated and the animals were reperfused for 24 h. At the end of reperfusion, rats were anaesthetized. The chest was opened, the coronary artery was re-occluded at the same location than previously performed and Evan's blue solution was injected through the apex to delineate the area at risk. The heart was excised, the left ventricle was cut into 6 slices and the infarct area was identified by 2,3,5-triphenyltetrazolium chloride (TTC) staining. The area at risk was identified as the non-blue region and expressed as a percentage of the left ventricle weight. The infarcted area was identified as the TTC positive zone and expressed as a percentage of area at risk.

Isolation of cardiac mitochondria and cytosols

Rats were euthanized by intraperitoneal injection of pentobarbital (150 mg/kg). Rat left ventricles were removed and immediately immersed in ice cold 0.9% NaCl, scissor minced and homogenized using a Polytron homogenizer in a cold buffer (4 °C, pH 7.4) containing: mannitol (220 mM), sucrose (70 mM), HEPES (10 mM) and EGTA (2 mM). The samples were further homogenized for 10 consecutive times using a Potter homogenizer at 1500 rev/min. The homogenates were then centrifuged at 1000 g for 5 min at 4°C to remove tissue debris and nuclei. The supernatants were centrifuged for 10 min at 10,000 g. The final pellets containing mitochondria were resuspended in the homogenization buffer with only 0.01mM of EGTA and were used immediately (evaluation of mitochondrial function) or frozen at – 80°C (western blot experiments and sterol determination). The supernatants were centrifuged at

100,000g for 60 min at 4°C. The pellets were discarded and the supernatants, corresponding to the cytosols, were frozen at – 80°C after determination of the protein concentrations (Pierce™ BCA Protein Assay Kit (23225, Thermofischer Scientific, Illkirch, France).
Testis and liver mitochondria were prepared using the same protocol without the Polytron homogenization step.

Evaluation of mitochondrial oxygen consumption and mitochondrial permeability transition pore opening

Oxygen consumption was measured with a Clark-type electrode (Hansatech Instruments Ltd, Norfolk, UK). Mitochondria (0.4 mg /mL) were incubated in a respiration buffer (100 mM KCl, 50 mM sucrose, 10 mM HEPES and 5 mM KH_2PO_4, pH 7.4 at 30°C). Respiration was initiated by addition of 2.5 mM pyruvate/malate. After 1 min, ATP synthesis was induced by addition of 1 mM ADP (ADP-stimulation respiration rate). ADP uptake was then inhibited by adding 1 µM carboxyatractyloside (substrate-dependent respiration rate). The respiratory control ratio (ADP-stimulation / substrate-dependent respiration rate) was then calculated.
mPTP opening was assessed by monitoring mitochondrial calcium retention capacity. Rat cardiac mitochondria were loaded with increasing concentrations of calcium until the load reached a threshold at which mitochondria underwent a fast process of calcium release, which was due to mPTP opening. Mitochondria (1 mg/mL), energized with 5 mM pyruvate/malate, were incubated in the respiration buffer supplemented with 1 mM Calcium Green-5N fluorescent probe (C3737, Invitrogen, Eugene, OR, USA). The reaction was started by addition of successive 10 µM Ca^{2+} pulses. The concentration of calcium in the extramitochondrial medium was monitored by means of a Jasco FP-6300 spectrofluorimeter (Jasco, Bouguenais, France) at excitation and emission wavelengths of 506 and 532 nm, respectively. The calcium signal was calibrated by addition to the medium of known calcium amounts.

Assessment of mitochondrial respiratory complex activities

The detailed methods of measurement of mitochondrial respiratory chain enzymatic activities are described in the supplementary file.

Measurement of superoxide anion production in myocardial mitochondria

Superoxide anion generation was assessed by measuring the rate of hydrogen peroxide production. This was determined fluorometrically by the oxidation of Amplex Red to fluorescent resorufin, coupled to the enzymatic reduction of hydrogen peroxide by horseradish peroxidase. Essentially, the superoxide generated in mitochondria is converted endogenously to hydrogen

peroxide and then measured by the assay. Briefly, Amplex Red (10 µM) and horseradish peroxidase (1 U/mL) were added to isolated mitochondria (0.2 mg/mL protein) in respiration buffer maintained at 30°C. The reaction was initiated by addition of the respiratory substrates (pyruvate/malate or succinate, 5 mM) in the presence or absence of 1 µM rotenone (inhibitor of complex I) and 1 µM antimycin A (inhibitor complex III). The subsequent increase in fluorescence was monitored over time using a fluorescence spectrometer (Perkin-Elmer SA LS 50B, excitation wavelength=563 nm; emission wavelength=587 nm).

Measurement of 4-hydroxynonenal

4-hydroxynonenal was measured using the Elabioscience competitive ELISA kit (Euromedex, Souffelweyersheim, France) according to the manufacturer's instruction. Briefly, the samples (0.2 mg protein) were added into a microplate pre-coated with 4-hydroxynonenal. After incubation with 4-hydroxynonenal antibody and with labeled horse radish peroxidase, substrate and stop solutions were added. The absorbance was measured at a wavelength of 450nm using Multiskan Sky (Thermo Scientific) plate reader, and the concentration of 4-hydroxynonenal was determined by comparing the optical density of the sample to the standard curve.

Isolation of primary adult rat cardiomyocytes

Left ventricular cardiomyocytes were isolated from *Tspo*$^{+/+}$ and *Tspo*$^{-/-}$ rats by an enzymatic technique. The rat was euthanized by intraperitoneal injection of pentobarbital (150 mg/kg) and the heart was excised. The heart was retrogradely perfused for 15 min at 37°C with a stock perfusion buffer bubbled with 95%O_2/5%CO_2 containing 133 mM NaCl, 4.7 mM KCl, 0.6 mM KH_2PO_4, 0.6 mM Na_2HPO_4, 1.2 mM $MgSO_4$, 12 mM $NaHCO_3$, 10 mM $KHCO_3$, 10 mM HEPES, 30 mM taurine, 0.032 mM phenol red, 5.5 mM glucose, 10 mM 2,3butanedionemonoxime pH 7.4 to wash out blood. After 2 min of perfusion, liberase (Blendzyme 10 mg/100 mL, Roche Applied Science, Mannheim, Germany), trypsin EDTA (14 mg/100 mL) and 12.5 µM Ca^{2+} were added to the buffer and the heart was perfused for approximately 13-15 min. The heart was placed into a beaker in the same buffer containing 10% bovine serum albumin pH 7.4 at 37°C to stop the digestion. Left ventricles were then cut into small fragments and cells isolated by stirring the tissue and successive aspirations of the fragments through a 10 mL pipette. After 10 min the supernatant was removed and the remaining tissue fragments were re-exposed to 10 mL of the same buffer. Then, the cells were suspended in the same buffer and Ca^{2+} was gradually added from 12.5 µM to 1 mM into an incubator at 37°C. Finally, the cardiomyocytes were suspended in culture medium M199 supplemented with 0.1% insulin-transferine-

selenium. The cells were seeded on 35 mm Petri dishes (150000/dish) pre-coated with 10 µg/mL sterilized laminin and incubated for 90 min before being used.

Evaluation of mitochondrial reactive oxygen species (ROS) production in living cardiomyocytes

Assessment of mitochondrial superoxide production in cardiomyocytes was performed using MitoSOX™ Red fluorescent probe which targets mitochondria and is oxidized by superoxide anion. Cells were washed with a Tyrode's buffer (in mM: NaCl 130; KCl 5; HEPES 10; $MgCl_2$ 1; $CaCl_2$ 1.8, glucose 5.6, pH 7.4 at 37 °C), loaded with 1 µM MitoSOX™ (30 min at 37°C) and then washed two times with the Tyrode solution.

The cardiomyocytes were placed into a thermostated (37°C) chamber (Warner Instruments, Hamden, CT), which was mounted on the stage of an IX-81 Olympus microscope and were paced to beat by field stimulation (5 ms, 0.5 Hz).

Cardiomyocytes were imaged with the Olympus IX-81 motorized inverted microscope equipped with a mercury lamp as a source of light for epifluorescence illumination and with a cooled camera (Hamamatsu ORCA-ER). MitoSOX™ Red fluorescence were excited at 520-550 nm and recorded at 580 nm. Images were acquired every 10 min from 0 to 60 min and analyzed using a digital epifluorescence imaging software (XCellence, Olympus, Rungis, France). Fluorescence was integrated over a region of interest (≈80 µm2) for each cardiomyocyte and a fluorescence background corresponding to an area without cells was subtracted. The global response was analyzed by averaging the fluorescence changes obtained from all the cardiomyocytes contained in a single field (20-30 cells).

Blood sample analysis

Blood was collected from 2, 6, and 12 months *Tspo*$^{+/+}$ and *Tspo*$^{-/-}$ rats. Rats were anesthetized with isoflurane (0.2 L/min O_2, 2.5% isoflurane) and blood were collected from the jugular vein. Serum lipid profile (total cholesterol, glycemia, HDL, free fatty acid, triglycerides) was performed with an automaton (Olympus AU 400) by Bichat Hospital's Biochemistry platform. Serum steroid hormones were measured with GC/MS by the mass spectrometry platform. Serum oxysterols measurements were carried with GC/MS.

Evaluation of CYP11A1 activity

The detailed methods of measurement of CYP11A1 activity in rat ventricular and testicular mitochondrial fractions using a cholesterol-resorufin probe and of synthesis of this probe are described in the supplementary file.

Metabolic tests

Metabolic tests were carried out according to Pitasi *et al*. [53]. Insuline tolerance tests were performed in 2, 6 and 12 months *Tspo*$^{+/+}$ and *Tspo*$^{-/-}$ rats. One week later, glucose tolerance tests were performed in the same rats. After 6 hours of fasting, rats received an intraperitoneal injection of insulin (1 UI/kg, 3% BSA in saline solution) or D-glucose (1 g/kg in saline). Glycaemia (fasting, 15, 30, 60, 90, 120 min after the injection) were measured with a hand-held glucometer (Accu-Chek Performa, Roche, France) through blood collected from tail vein. The area under the curve (AUC) were calculated using Graphpad Prism. The AUC values for the glucose tolerance tests were normalized as follows: AUC = totalAUC - (fasting glycaemia * 120). The area over curve (AOC) for the insulin tolerance tests were calculated as follows: AOC = (fasting glycaemia * 120) - totalAUC.

Western Blot analysis

After denaturing proteins at 90°C for 5 minutes, a total of 40µg of protein samples were loaded onto 8-16% Mini-PROTEAN® TGX™ Precast Gel (4561104, Bio-Rad) and separated by SDS-PAGE electrophoresis and then transferred to PVDF membranes. Next, membranes were blocked with a 5% skim milk solution for 1h30 at room temperature. After, they were probed with antibodies against CYP11A1 (1/250, sc18043, Santa Cruz Biotechnologies), CYP27A1 (1/250, sc14835, Santa Cruz Biotechnologies), TSPO (1/1000, ab154878, Abcam), STAR 37-kDa (1/1000, MBS3223061, Cliniscience), STAR 30-kDa (1/1000, ab58013, Abcam), VDAC (1/1000, 4866, Cell Signaling), superoxide dismutase 2 (SOD2; 1/1000, ab13533, Abcam), cytochrome C oxidase (COX-IV; 1/2000, 4844, Cell Signaling), β-actin (1/2000, 4970, Cell Signaling) and glyceraldehyde 3-phosphate dehydrogenase (GAPDH; 1/1000, 5174, Cell Signaling). Membranes were then incubated with horseradish peroxidase conjugated secondary antibodies, anti-mouse (1/5000, 7076, Cell Signaling), and anti-rabbit (1/5000, 7074, Cell Signaling). Finally, blots were revealed with ECL Western Blotting detection reagents (Amersham, GERPN2209, Sigma-Aldrich). The signal intensities for specific bands on the Western Blot were quantified using Image J software (1.30v - National Institute of Health).

Immunohistochemistry

Formalin-fixed rat left ventricles were embedded in paraffin and cross-sections (5 µm thickness) were performed using a rotary microtome. Briefly, after rehydration, antigen retrieval was performed with heated citrate buffer. After endogenous peroxidase antigen blocking (H_2O_2 3% 15 min) followed by antigen blocking (1h, 30% goat serum), sections were incubated with primary antibodies (TSPO, goat ab154878 1:180 - overnight at 4 °C). The following day sections were washed and incubated with a horseradish peroxidase-conjugated secondary antibody (Abcam; ab97051 1:200) for 30 minutes at room temperature. The sections were washed again and incubated with 3,3'-diaminobenzidine (DAB; Vector Laboratories) under visual observation until the signal appears. The reaction was stopped by immersing slides in water. Images were acquired using an inverted optical microscope (Axioplan 2, Zeiss) at x400 magnification.

Analysis of mRNA expression

Total RNAs were extracted from left ventricles (sham or ischemia-reperfused) with a column extraction kit (Maxwell® 16 LEV simplyRNA Tissue, Promega) following the manufacturer's instructions. Reverse transcription was performed using the AffinityScript qPCR cDNA Synthesis kit (Agilent). Quantitative polymerase chain reaction (qPCR) was performed using TaqMan Gene Expression assays (Thermo Fischer Scientific) and TaqMan primers (FAM) for *Tspo* (Rn00560892-m1), *Star* (Rn00580695-m1), *Cyp11A1* (Rn00568733-m1), *Cyp27A1* (Rn00710297-m1) and *Rplp0* (Rn03302271-gH) from Thermo Fisher Scientific. Amplification reactions were carried out using a 7000 Real-Time PCR system (Applied Biosystems). Gene expression was assessed by the comparative CT (ΔΔCT) method, with *Rplp0* as the reference gene.

Determination of cholesterol and oxysterol levels

Sterol and oxysterol measurements were performed on cytosolic and mitochondrial extracts. After extraction, they were measured by gas chromatography – isotope dilution mass spectrometry. The details are described in the online supplementary file.

Evaluation of cardiac hypertrophy

To assess cardiac hypertrophy, formalin-fixed rat left ventricles were embedded in paraffin and cross-sections (5 µm thickness) were performed using a rotary microtome. sections were rehydrated and incubated for 45 minutes at room temperature with 10 µg/mL Alexa488-

conjugated wheat germ agglutinin (WGA; Invitrogen). Slides were then mounted using glycerol and containing 4′,6-diamidino-2-phenylindole (DAPI). Images were acquired using an inverted fluorescent microscope at x200 magnification (AxioImager M2, Zeiss) and analyzed with the Image J software. Cardiac hypertrophy was also assessed by measuring the ratio between the weight of the left ventricle and the body weight of the animals.

Echocardiography

Rats were lightly anesthetized with ketamine (60 mg/kg) and xylazine (6 mg/kg), given intraperitoneally, before echocardiography protocol. A 10 MHz ultrasound probe was used with a digital ultrasound system (Vivid 7, GE Medical Systems, Little Chalfont, UK). A trained operator performed echocardiograms and analysis.

The left ventricular (LV) end-diastolic diameter (LVEDD), as the thickness of the interventricular septum (IVSd), and posterior wall (LVPWd) in the end-diastole were determined on M-mode echocardiography in the parasternal short-axis view at the level of papillary muscles. Transmitral flow velocities (E and A velocities and their ratio) were measured by pulse wave Doppler in the apical 4-chamber view.

LV fractional shortening (LV FS) was calculated as (LVEDD-LVESD)/LVEDD x 100, LVESD is LV end-systolic diameter. Heart rate (HR) was measured between two diastolic cycles on the M-mode image obtained in the parasternal short-axis view at the level of papillary muscles. LV ejection fraction (EF) was calculated using Teicholz formula: EF (%) = (EDV-ESV)/EDV*100, where EDV (end-diastolic volume) = $[7/(2.4+LVEDID)]*LVEDID^3$ and ESV (end-systolic volume) = $[7/(2.4+LVESID)]*LVESID^3$. LVEDID and LVESID were LV internal diameter in the end-diastole and end-systole, respectively measured using the cine loop of the parasternal short-axis view at the level of papillary muscles.

Statistical analysis

Rats were randomly assigned to the various treatment groups and experiments were performed in parallel with rats from each strain. No formal exclusion or inclusion criteria for animals were applied (beside the inclusion of male rats only). No statistical method was used to predetermine sample size. Sample sizes were chosen based on our previous experience and corresponds to standards in the field. Sample sizes are indicated in the corresponding figure legend. No animals were excluded after randomisation except procedure failure.

The experimenter was blind when he analysed histological immunostaining and performed echocardiographic experiments and sterol, steroidogenic hormone and lipid blood level dosages.

Statistical analysis was performed with GraphPad Prism 9.1.2 (Graph Pad Software, USA). Data were presented as the means ± standard error of mean (SEM). Statistical significance of differences between two groups was determined using an unpaired two-tailed t-test. Significant differences between more than two groups were evaluated by one-way or two-way ANOVA analysis followed by the multi-comparison post-test recommended by GraphPad Prism if ANOVA produced a significant value of F ($p < 0.05$). Statistical parameters and significance are reported in the figures and the figure legends.

Results

The inhibition of cholesterol synthesis reduces mitochondrial cholesterol accumulation and protects mitochondria against myocardial ischemia-reperfusion injury.

To reduce cholesterol biosynthesis, we used pravastatin, an inhibitor of 3-hydroxy-3-methyglutaryl-CoA reductase, which blocks the mevalonate pathway. Male Wistar rats were treated or not with pravastatin (10 mg/kg/day per os, 3 days) and submitted or not to 30 min of coronary artery occlusion followed by 15 min of reperfusion. After sacrifice, the hearts were removed and cytosols and mitochondria were isolated from the ischemic area to measure cholesterol and oxysterol concentrations.

Fig. 2a shows that the reperfusion of an ischemic myocardium produced an increase in mitochondrial cholesterol concentration. A similar result was obtained in the corresponding cytosols (Fig. 2b) indicating that reperfusion promotes a global cellular accumulation of cholesterol that can result from a cellular stimulation of synthesis and/or an efflux of cholesterol from the blood compartment. This was associated with a significant increase in oxysterol contents in both mitochondria and cytosols (Fig. 2d and 2e).

In sham animals, pravastatin did not modify cytosolic (Fig. 2b) but slightly decreased mitochondrial cholesterol (Fig. 2a). We did not observe any effect of pravastatin on the concentrations of oxysterols measured in cardiac mitochondria isolated from sham rats (Fig 2d). In cardiac cytosols pravastatin treatment did not modify the concentrations of 7α-hydroxycholesterol and 7-ketocholesterol but, intriguingly, increased the concentration of 7β-hydroxycholesterol (Fig. 2e).

When rats were subjected to ischemia-reperfusion, pravastatin limited the enhancement of cholesterol in the cytosol and abolished its accumulation in the mitochondria (Fig. 2a and 2b).

This was associated with strong inhibition of oxysterol production in the mitochondria whereas no decrease could be observed in the cytosols (Fig. 2d and 2e). It should be noted that pravastatin treatment did not lower serum cholesterol whatever the group of rats (Fig. 2c).

We next examined the concomitant effect of pravastatin treatment on mitochondrial function. Along with the reduction in mitochondrial cholesterol and oxysterols accumulation, pravastatin significantly improved oxidative phosphorylation as demonstrated by the increase in both ADP-stimulated respiration (state 3) and the respiratory control ratio (+48.4% versus ischemia-reperfusion). Pravastatin also decreased the sensitivity of mitochondria to mPTP opening as demonstrated by their increased capacity to retain calcium (+52.4% versus ischemia-reperfusion) (Table 1).

3.2. Cardiac mitochondrial cholesterol accumulation is not mediated by the inhibition of cholesterol catabolism during ischemia-reperfusion

Two CYP are responsible for the catabolism of cholesterol in mitochondria: CYP11A1 and CYP27A1. They are located to the matrix side of the inner mitochondrial membrane and convert cholesterol to pregnenolone and 27-hydroxycholesterol, respectively. In heart mitochondria, the presence and/or the role of these proteins remains a source of questions [7]. As illustrated in Fig. 3a, Western Blot experiments confirmed the presence of CYP11A1 in cardiac mitochondria, which is at the limit of detection when comparing the content observed in the testis on the same gel (Fig. 3b). Original western blots of all the figures are shown in the supplementary file. To go further, we next analyzed the activity of the enzyme in isolated mitochondria using the fluorescent probe cholesterol-resorufin. We synthesised a CYP11A1 fluorescent probe in which a resorufin molecule was conjugated to the side chain of cholesterol (see supplementary file). CYP11A1 cuts the cholesterol side chain and releases the fluorescent resorufin, which can be measured at 590 nm. In accordance with the expression of CYP11A1, the activity of the enzyme in the heart was very low compared to that observed in the testis (Fig. 3c). This is corroborated by the fact that we were unable to detect pregnenolone using isotope dilution mass spectrometry in isolated heart mitochondria (results not shown). Western blot experiments allowed also to reveal the presence of CYP27A1 in rat isolated cardiac mitochondria (Fig. 3a) which, as CYP11A1 compared to testis, was very low compared to liver (Fig. 3b). This had not been established before and this was supported by the presence of 27-hydroxycholesterol inside cardiac mitochondria (0.0442±0.0073 µg/mg protein; n=15 different preparations). Then, we examined the effect of ischemia-reperfusion on both cytochromes. Fig. 3a shows that protein and mRNA expressions of both cytochromes were not affected after ischemia-reperfusion nor was the activity of CYP11A1 (Fig. 3c). In the same way, the mitochondrial concentration of 27-hydroxycholesterol significantly increased

after ischemia-reperfusion (from 0.0442±0.0073 (n=15) to 0.071±0.004 (n=10) µg/mg protein) ruling out an inhibition of CYP27A1 activity. These results tend to indicate that the accumulation of mitochondrial cholesterol was not a consequence of a cholesterol metabolism deficiency during ischemia-reperfusion.

3.3. Cardiac cholesterol accumulation at reperfusion is related to an increase in mitochondrial STAR but not in TSPO levels.

The accumulation of mitochondrial cholesterol at reperfusion can also be due to an enhancement of the intra-mitochondrial transport of cholesterol. Therefore, we investigated two proteins considered as critical for this transport, STAR and TSPO, even if the role of the latter in steroid organs was discussed [40,49]. To assess the role of these proteins, we examined their mitochondrial levels in the absence or in the presence of ischemia-reperfusion in isolated cardiac cytosols and mitochondria. TSPO was expressed in cardiac mitochondria but no significant change in protein and mRNA expression could be observed after ischemia-reperfusion (Fig. 3d and 3g). This is in agreement with our previous study indicating that ischemia-reperfusion did not change the level of TSPO when it was probed with the specific TSPO ligand PK11195 [37]. As illustrated in Fig. 3e, STAR was expressed as a 37-kDa form in the cytosols isolated from rat hearts. After ischemia-reperfusion, the level of 37-kDa STAR decreased by 65 % in the cytosol (Fig. 3e). This decrease was associated with a strong decrease in the expression of mRNA (Fig. 3g). Concomitantly, we observed the apparition of a 30-kDa form of STAR in mitochondria (Fig. 3f).

3.4. The effect of pravastatin on mitochondrial sterol accumulation is associated with the inhibition of mitochondrial STAR processing.

As pravastatin limited the accumulation of cholesterol and oxysterols in the mitochondria at reperfusion (Fig. 2a and 2d), we wondered whether the limitation of mitochondrial STAR processing could be involved in this effect. Thus, according to the protocol previously described, we examined the effect of the administration of pravastatin on the induction of the mitochondrial STAR processing. Fig. 4a confirmed the mitochondrial accumulation of STAR 30-kDa at reperfusion. It was totally inhibited by pravastatin administration (Fig. 4a).

3.5. The TSPO ligand 4'-chlorodiazepam inhibits STAR mitochondrial processing.

We previously demonstrated that TSPO ligands inhibited oxysterol formation by reducing the accumulation of cholesterol in the mitochondrial matrix at reperfusion [51]. We reasoned that

549 this effect could be caused by the limitation of STAR mitochondrial membrane processing.
550 Thus, we examined the effect of the administration of 4'-chlorodiazepam on mitochondrial
551 STAR accumulation at reperfusion. When administrated before reperfusion, 4'-
552 chlorodiazepam greatly limited STAR mitochondrial levels (Fig. 4b). As previous data have
553 suggested that the effect of TSPO ligands could be independent from TSPO [26,63], we
554 wanted to ascertain the involvement of TSPO in the effect of 4'-chlorodiazepam. To do that,
555 we used *Tspo*$^{-/-}$ rats.
556
557 *3.6. Tspo deletion reduces mitochondrial sterols accumulation without altering mitochondrial*
558 *function in rats subjected to ischemia-reperfusion.*
559
560 Fig. 5 shows the impact of *Tspo* deletion on mitochondrial sterol content. In sham animals,
561 *Tspo* deletion did not alter the level of mitochondrial cholesterol (Fig. 5a) but strongly
562 decreased the level of mitochondrial oxysterols (Fig. 5b-g). These oxysterols are known to be
563 formed by auto-oxidation, except 25-hydroxycholesterol which has also be found to result from
564 enzymatic conversion of cholesterol. This decrease in oxysterol content was not observed in
565 cardiac cytosols (Table 2) indicating that it could result from a limitation of mitochondrial ROS
566 production in *Tspo*$^{-/-}$ mitochondria. To ascertain this hypothesis, we compared the basal level
567 of mitochondrial superoxide generation in cardiomyocytes isolated from *Tspo*$^{+/+}$ and *Tspo*$^{-/-}$ rats
568 and we measured lipid peroxidation in cardiac mitochondria isolated from *Tspo*$^{+/+}$ and *Tspo*$^{-/-}$
569 rats. Fig. 6a and 6b provide direct evidence of this hypothesis. *Tspo* deletion limits
570 mitochondrial superoxide anion production over time in paced cardiomyocytes, as
571 demonstrated by the lower MitoSOX fluorescence in *Tspo*$^{-/-}$ cardiomyocytes (Fig. 6a), and
572 decreases the concentration of the lipid peroxidation product 4-hydroxynonenal in
573 mitochondria isolated from *Tspo*$^{-/-}$ rats (Fig. 6b). This decrease was not observed in the
574 corresponding cytosols (Fig. 6b). Mitochondrial superoxide anions can be produced by the
575 electron transport chain through electron leak and complexes I and III are recognized as the
576 major sites of production [67]. Therefore, we analyzed the rate of superoxide production by
577 measuring the rate of hydrogen peroxide production in cardiac mitochondria isolated from
578 *Tspo*$^{+/+}$ and *Tspo*$^{-/-}$ rats. We found that it was similar whatever the substrate used to induce
579 respiration, excluding a participation of the mitochondrial transport chain in this effect (Fig. 6c).
580 This in accordance with the activity of mitochondrial transport chain complexes as no difference
581 was found between *Tspo*$^{+/+}$ and *Tspo*$^{-/-}$ rats when the activity of each complex was measured
582 separately (Online Fig. S5). In the same way, the expression of superoxide dismutase 2, the
583 main mitochondrial antioxidant enzyme, was not altered in deleted animals, ruling out a role of
584 this enzyme in the decrease in superoxide anions production (Fig. 6d). We also analyzed the
585 expression of VDAC because the interaction between TSPO and VDAC was shown to

modulate oxidative stress [20,38]. Our results show that *Tspo* deletion did not alter the expression of VDAC (Fig. 6d).

We did not observe any consequences of these sterol alterations in sham animals on cardiac mitochondrial function (Fig. 7). When mitochondria were extracted from *Tspo*$^{+/+}$ and *Tspo* $^{-/-}$ rats, the yield of extraction, determined by measuring the concentration of proteins in the mitochondrial pellet per g of cardiac tissue, was identical, reflecting a similar number of mitochondria in hearts (Fig. 7a). Similarly, *Tspo* deletion did not affect mitochondrial respiration or oxidative phosphorylation as illustrated by the similar V3 (Fig. 7b) and respiratory coefficient rate (Fig. 7c) values and did not alter the capacity of mitochondria to retain calcium, a marker of the mitochondrial membrane impermeability (Fig. 7d). *Tspo* deletion being without consequence on basal cardiac mitochondrial function, we assumed that the effect of *Tspo* deletion could appear following a cardiac stress.

Therefore, rats of both genotypes were subjected to cardiac ischemia-reperfusion and mitochondrial sterols and function were assessed. Ischemia-reperfusion induced an increase in mitochondrial cholesterol and oxysterols in *Tspo*$^{+/+}$ animals (Fig. 5) as previously described [41,42,51]. It should be noted that these results were obtained in Sprague Dawleys animals (the strain in which *Tspo*$^{-/-}$ rats were generated) and confirmed all our previous results using Wistar animals.

Tspo deletion did not prevent but blunted cholesterol and oxysterol accumulation following ischemia-reperfusion (Fig. 5). However, this decrease in sterols had no consequences on mitochondrial parameters, which remained similar between *Tspo*$^{+/+}$ and *Tspo*$^{-/-}$ rats (Fig. 7a-d). As a result, no difference infarct size was observed in rats subjected to 30 min ischemia followed by 24-hour reperfusion (Fig. 7e).

3.7. Deletion of Tspo abolishes the effect of 4'-chlorodiazepam on mitochondrial STAR processing and cholesterol accumulation without effect on STAR 37-kDa.

Tspo$^{-/-}$ rats being generated from a different strain (Sprague Dawleys animals) than that used in all our previous experiments, we assessed the effect of 4'-chlorodiazepam on mitochondrial STAR in Sprague Dawleys *Tspo*$^{+/+}$ rats subjected to ischemia-reperfusion before analyzing its effect in *Tspo*$^{-/-}$ rats. Ischemia-reperfusion induced an increase in mitochondrial STAR 30-kDa level, which was inhibited by 4'-chlorodiazepam administration (Fig. 8a). Similarly, 4'-chlorodiazepam prevented mitochondrial cholesterol accumulation (Fig. 8b) confirming the results obtained with Wistar rats. These data legitimized the use of Sprague Dawleys *Tspo*$^{-/-}$ rats.

Fig. 8c shows that the mitochondrial enhancement of STAR 30-kDa caused by ischemia-reperfusion persisted in *Tspo*$^{-/-}$ rats, demonstrating a TSPO-independent mitochondrial processing of STAR. Nevertheless, *Tspo* deletion abolished the effect of 4'-chlorodiazepam, the administration of the drug being unable to prevent cholesterol accumulation (Fig. 8d), to inhibit STAR 30-kDa enhancement in mitochondria (Fig. 8c) and to improve mitochondrial functional parameters (Fig. 7) after ischemia-reperfusion. This confirms the role of TSPO in the mitochondrial protecting effect of 4'-chlorodiazepam.

As it was shown that *Tspo* depletion induced an alteration of the level of STAR 37-kDa in Leydig tumor cells [27], we wondered whether global deletion of *Tspo* would alter the STAR 37-kDa cytosolic form. Cardiac ischemia-reperfusion in *Tspo*$^{+/+}$ Sprague Dawley rats confirmed the decrease in the level of STAR 37-kDa in cardiac cytosols (Fig. 8e) and this decrease was not altered by 4'-chlorodiazepam (Fig. 8f). Similar results were observed in *Tspo*$^{-/-}$ rats, *i.e.*, the decrease in cytosolic STAR 37-kDa level observed after ischemia-reperfusion was preserved and the administration of 4'-chlorodiazepam was without effect (Fig. 8g and 8h).

4. Discussion

Early reperfusion of an ischemic myocardium induces an accumulation of mitochondrial cholesterol and oxysterols, which is potentiated by hypercholesterolemia [41,51]. In this setting, administration of TSPO ligands prevented mitochondrial sterol accumulation, protected mitochondrial function and reduced infarct size [45,51]. This protective effect is preserved during hypercholesterolemia [41]. This makes controlling mitochondrial cholesterol concentration an interesting strategy to protect mitochondria during myocardial ischemia-reperfusion and particularly in hypercholesterolemic conditions that are known to amplify cellular injury and to impede cardioprotective mechanisms [1]. In the present study, we provide evidence that inhibiting cholesterol synthesis protects mitochondrial function during myocardial ischemia-reperfusion independently from any blood level lowering effect. We also provide novel findings that extend the understanding on the mechanisms responsible for mitochondrial cholesterol entry and accumulation during myocardial ischemia-reperfusion.

An important step of this study was to rule out the possibility of a defect in mitochondrial cholesterol catabolism that could explain mitochondrial cholesterol accumulation. We clearly established in the rat heart the presence of the cytochromes, which are responsible for cholesterol catabolism in mitochondria, *i.e.,* CYP11A1 and CYP27A1. To the best of our knowledge, only one study described the presence of CYP11A1 in the heart (human heart) [68] and that of CYP27A1 was unknown [7]. CYP11A1 constitutes an essential step for the formation of steroid hormones and its presence suggests a possible *de novo* cardiac

steroidogenesis although we cannot yet detect pregnenolone. CYP27A1 is considered as a major mechanism for cholesterol efflux from peripheral tissues, as emphasized by Babiker *et al.* [4] showing that patients with CYP27A1 gene mutations do not secrete 27-oxygenated products of cholesterol in peripheral macrophages. The role of these cytochromes in cardiovascular physiology and physiopathology is largely unexplored. We demonstrate that they are very poorly expressed in the rat heart compared to reference organs but, most importantly, that their expression and activity are not modified after reperfusion. These results provide evidence that the increased influx of cholesterol and not an alteration of its mitochondrial metabolism is responsible for its mitochondrial accumulation during myocardial ischemia-reperfusion.

To investigate the mechanisms explaining mitochondrial accumulation of cholesterol, we reduced cholesterol synthesis using pravastatin that inhibits 3-hydroxy-3-methyglutaryl-CoA reductase and thus acts upstream of mitochondria. We chose this statin because it is freely soluble in water and thus easy to use in animal models. As previously observed [18,33], pravastatin treatment did not lower serum cholesterol in our experimental conditions. This is in accordance with studies indicating that pravastatin only exerts a hypocholesterolemic effect in dyslipidemic animal models [12,15,52]. Here, pravastatin did not alter the concentration of sterols in cardiac cytosols isolated from sham rats, which is in line with this hypothesis. The brevity of the pravastatin treatment (3 days) can also participate to this lack of effect. We observed, however, an increase in 7β-hydroxycholesterol in the cytosols of sham animals. This increase was unexpected but was associated with the inversion of the ratio 7-ketocholesterol/7β-hydroxycholesterol. A balance exists between the circulating and the tissue levels of 7-ketocholesterol and 7β-hydroxycholesterol *in vivo* and this balance is regulated by the 11β-hydroxysteroid dehydrogenase type 1 [23]. The reduction of 7-ketocholesterol in 7β-hydroxycholesterol is stereospecific and this enzyme is present in the rat heart [66]. We can assume that pravastatin treatment favors the formation of 7β-hydroxycholesterol but this needs to be confirmed.

During ischemia-reperfusion, pravastatin limited the cytosolic concentration of cholesterol but not of oxysterols. This might be the consequence of an insufficient decrease in cytosolic cholesterol, which did not reach the threshold needed to significantly reduce oxysterol content. In contrast, pravastatin strongly inhibited cholesterol and oxysterol accumulation in the mitochondria, and restored the capacity of mitochondria to synthetize ATP and to resist to mPTP opening. These are key factors involved in cell protection and they may strongly contribute to the cardioprotective effect of pravastatin. These novel results show that decreasing mitochondrial cholesterol by inhibiting cholesterol metabolism protects mitochondria from ischemia-reperfusion injury. However, it should be kept in mind that short

pravastatin treatment can initiate other mechanisms concomitantly to its sterol-lowering action that can also contribute to its protective effect [6].

Importantly, we also identified a mechanism involved in the accumulation of cholesterol and oxysterols into mitochondria during myocardial ischemia-reperfusion. We demonstrated a mitochondrial targeting and processing of STAR 37-kDa leading to a mitochondrial STAR 30-kDa mature protein. The mitochondrial accumulation of STAR 30-kDa and sterols during reperfusion are blocked by both the inhibition of cholesterol synthesis by pravastatin and the TSPO ligand 4'-chlorodiazepam. In addition, 4'-chlorodiazepam was ineffective to inhibit ischemia-reperfusion induced STAR import and cholesterol accumulation and to improve mitochondrial functional parameters in *Tspo*$^{-/-}$ rats. All these findings clearly demonstrate that a functional interaction exists between STAR and TSPO in cardiac cells as observed in Leydig cells [27]. They also validate that 4'chlorodiazepam acts through its binding to TSPO.

It should also be stressed that TSPO is not mandatory for mitochondrial STAR import and cholesterol accumulation, as both processes were not abolished in *Tspo*$^{-/-}$ rats in basal conditions. This is consistent with data obtained on steroidogenic organs where TSPO appears non-essential for low-flux steroidogenesis [16]. This hypothesis is supported by the data showing no variation of cardiac phenotypes between *Tspo*$^{+/+}$ and *Tspo*$^{-/-}$ rats. It was suggested that adaptive mechanisms could take place to compensate for the lack of TSPO [16,48]. This raises questions concerning the role of TSPO in the heart *in vivo* since it must bind a ligand to exert an action. Moreover, in the heart, TSPO appears as a spectator unable to control STAR processing but its absence limits cholesterol movements during reperfusion. This suggests that the interaction between STAR and TSPO is necessary for an efficient transport of mitochondrial cholesterol particularly when its strong activation is needed.

Our results also indicate that a role of TSPO in the heart may be a control of mitochondrial ROS production. Indeed, we demonstrated that TSPO deletion attenuates mitochondrial superoxide production in primary cardiomyocytes and lipoperoxidation in isolated mitochondria. This is associated with a reduction of cardiac mitochondrial oxysterols, which can be the consequence of a reduction of available ROS in mitochondria leading to a decrease in cholesterol oxidation. This is in accordance with studies suggesting a relationship between TSPO, ROS levels and oxidative stress [8,39]. This is in line with recent data, which report significantly low ROS levels in the epithelial human breast cancer cell line MDA when TSPO is down-regulated [14] and an accumulation of ROS to limit the efficiency of mitochondrial autophagy when TSPO expression is enhanced [21]. So far, we did not determine the cause of this decrease in mitochondrial superoxide anion generation but we have excluded an alteration of the respiratory chain and of the expression of SOD2. The interaction between

TSPO and VDAC, which was shown to modulate ROS production [20,38] and is absent in deleted animals, could be involved in this effect but this hypothesis needs additional experiments to be confirmed. Moreover, the effect of 4'-chlorodiazepam treatment on mitochondrial ROS generation in wild-type and knock-out animals is lacking and the control of ROS production by TSPO deserves further investigations in the future.

We also observed that myocardial ischemia-reperfusion at its acute phase does not induce changes in TSPO expression. This is in line with data indicating that modulation of TSPO expression probably requires chronic processes and is most of the time observed during chronic pathologies such neurodegenerative, neuroinflammatory, and neuropsychiatric diseases [10,44], cerebral ischemia [56] or diabetic cardiomyopathy [22].

Our study highlights the role of STAR as a key protein during the reperfusion of an ischemic myocardium. STAR probably answers to the metabolic needs of the cells but acts as a deleterious agent stimulating cholesterol accumulation and generation of oxysterols, which are harmful for mitochondria during reperfusion. In contrast, Anuka *et al.* [2] demonstrate a cardioprotective role of STAR in cardiac fibroblasts in post-infarction conditions caused by an expression of the protein showing antiapoptotic activity, thus unrelated to the traditional role of the protein in steroidogenesis as recently described [19]. This apparent discrepancy could be explained by different physiopathological setting as Anuka *et al.* [2] used a permanent occlusion mouse model with investigations performed more lately during reperfusion (3 days). We cannot exclude the possibility for STAR to possess two properties in stress events, a short-term cholesterol transport property and a long-term antiapoptotic effect.

Another point to be studied is the characterization of the cellular signaling pathway leading to the accumulation of mitochondrial cholesterol during cardiac ischemia-reperfusion. In steroid organs and brain, the cyclic AMP-dependent protein kinase (PKA) is a primary modulator of StAR and TSPO activity and facilitates mitochondrial cholesterol transport [11,57]. In the heart, PKA has been involved in both the harmful effect of ischemia-reperfusion and the protection effect conferred by preconditioning. Moreover, specific isoforms of phosphodiesterases, cAMP-degrading enzymes regulating the cellular level of cAMP and thus PKA activity, are targets to protect the heart against ischemia-reperfusion injury [13], and modulate mitochondrial function [34]. It will be interesting to know if phosphodiesterases/PKA signalling pathways participate in the control of mitochondrial cholesterol accumulation during cardiac ischemia-reperfusion.

More generally, this work shows that cholesterol, by means of a TSPO/STAR interaction, participates in the changes in lipid cardiac profile and, thus, in the lipotoxicity contributing to cardiac ischemia-reperfusion injury [61]. Other mitochondrial mechanisms such as the

increase in carnitine palmitoyl transferase 1A [35] have been recently shown to contribute to this lipotoxicity. Further studies are required to explore a possible interaction between these mechanisms since regulating mitochondrial metabolism is a promising strategy to limit the extent of myocardial ischemia-reperfusion injury.

Limitations and future perspective of the study

This study has several limitations: 1) the use of only male rats is not consistent with contemporary standards on sex as a biological variable and sex is an important variable to take into account. We used male rats because cardiovascular studies are generally performed with male, especially because female hormones have cardioprotective properties [17] but also because all our previous studies were performed with male animals; 2) some experiments were performed with a rather low number of samples which might limit the statistical analysis power; 3) the present study focuses on subsarcolemmal mitochondria. Future studies will be aimed at investigating whether interfibrillar mitochondria, which differ in their functional responses and protein content, behave in the same way with respect to TSPO and Star during ischemia-reperfusion. 4) future works are needed to visualize the increase in mitochondrial cholesterol uptake and, thus, to confirm the causal role of mitochondrial sterol accumulation in ischemia-reperfusion injury. This can be done in cardiomyocytes subjected to hypoxia-reoxygenation when a suitable cholesterol probe will be available to monitor mitochondrial cholesterol uptake.

Conclusions

In conclusion, the present study highlights STAR translocation to the mitochondria and its coupling with TSPO to import cholesterol and to promote oxysterol formation during ischemia-reperfusion. This interaction regulates mitochondrial homeostasis and play a key role during mitochondrial injury.

Acknowledgement

We thank Pr V Papadopoulos (University of Southern California, USA) for providing two pairs of heterozyte TSPO deleted rats, which allowed us to develop a colony. We also thank him for helpful advices concerning the synthesis and the use of the fluorescent probe cholesterol-resorufin and for rereading the manuscript. The authors are greatly indebted to the Plateforme de Biochimie du Centre de Recherche sur l'Inflammation (Hopital Bichat, Paris, France) for blood analyses. We thank the Imagery platform of IMRB for histological samples preparation and the Animal Facility of IMRB for animal care. We also thank Lucien Sambin and Alain Bizé for their help during echocardiographic exams.

Author contribution statement

VL, MR, SP, BG and DM contributed to the experimental design; JB, SL, JM, JBS, NE, FG, LAB, CT, FV, CC and DM conducted the experiments; JB, SL, JM, SP, DM performed data analysis; SP, BG and DM wrote or contributed to the writing of the manuscript with input from all co-authors. All authors have read and approved the content, and agree to submit for consideration for publication in the journal.

Fundings

This work was supported by the Fondation de France [grant number 2018-00086493]. Juliette Bréhat and Julien Musman were supported by doctoral grants from the Ministère de l'enseignement Supérieur, de la Recherche et de l'Innovation.

Availability of data and materials

Availability of data and material Data are available from the corresponding author on reasonable request.

Declarations

Conflict of interests

On behalf of all authors, the corresponding author states that there is no conflict of interest.

Ethics approval

All animal procedures used in this study were conformed to the Directives of the European Parliament (2010/63/EU-848 EEC). The experimental protocols were reviewed and approved (APAFIS13504#-201820130912402v3 and APAFIS#23908-2020012712028279 v4) by the local Ethic Committee Cometh (Afssa/ENVA/UPEC, N° 16).

References

1. Andreadou I, Iliodromitis EK, Lazou A, Görbe A, Giricz Z, Schulz R, Ferdinandy P (2017) Effect of hypercholesterolaemia on myocardial function, ischaemia-reperfusion injury and cardioprotection by preconditioning, postconditioning and remote conditioning. Br J Pharmacol 174:1555-1569 doi: 10.1111/bph.13704

2. Anuka E, Yivgi-Ohana N, Eimerl S, Garfinkel B, Melamed-Book N, Chepurkol E, Aravot D, Zinman T, Shainberg A, Hochhauser E, Orly J (2013) Infarct-induced steroidogenic acute regulatory protein: a survival role in cardiac fibroblasts. Mol Endocrinol 27:1502-1517 doi: 10.1210/me.2013-1006

3. Artemenko IP, Zhao D, Hales DB, Hales KH, Jefcoate CR (2001) Mitochondrial processing of newly synthesized steroidogenic acute regulatory protein (StAR), but not total StAR, mediates cholesterol transfer to cytochrome P450 side chain cleavage enzyme in adrenal cells. J Biol Chem 276:46583-46596 doi: 10.1074/jbc.M107815200

4. Babiker A, Andersson O, Lund E, Xiu RJ, Deeb S, Reshef A, Leitersdorf E, Diczfalusy U, Björkhem I (1997) Elimination of cholesterol in macrophages and endothelial cells by the sterol 27-hydroxylase mechanism. Comparison with high density lipoprotein-mediated reverse cholesterol transport. J Biol Chem 272:26253-26261 doi: 10.1074/jbc.272.42.26253

5. Banati RB, Middleton RJ, Chan R, Hatty CR, Kam WW, Quin C, Graeber MB, Parmar A, Zahra D, Callaghan P, Fok S, Howell NR, Gregoire M, Szabo A, Pham T, Davis E, Liu GJ (2014) Positron emission tomography and functional characterization of a complete PBR/TSPO knockout. Nat Commun 5:5452 doi: 10.1038/ncomms6452

6. Bao N, Minatoguchi S, Kobayashi H, Yasuda S, Kawamura I, Iwasa M, Yamaki T, Sumi S, Misao Y, Arai M, Nishigaki K, Takemura G, Fujiwara T, Fujiwara H (2007) Pravastatin reduces myocardial infarct size via increasing protein kinase C-dependent nitric oxide, decreasing oxyradicals and opening the mitochondrial adenosine triphosphate-sensitive potassium channels in rabbits. Circ J 71:1622-1628 doi: 10.1253/circj.71.1622

7. Barau C, Ghaleh B, Berdeaux A, Morin D (2015) Cytochrome P450 and myocardial ischemia: potential pharmacological implication for cardioprotection. Fundam Clin Pharmacol 29:1-9 doi: 10.1111/fcp.12087

8. Batoko H, Veljanovski V, Jurkiewicz P (2015) Enigmatic Translocator protein (TSPO) and cellular stress regulation. Trends Biochem Sci 40:497-503 doi: 10.1016/j.tibs.2015.07.001

9. Bøtker HE, Cabrera-Fuentes HA, Ruiz-Meana M, Heusch G, Ovize M (2020) Translational issues for mitoprotective agents as adjunct to reperfusion therapy in patients with ST-segment elevation myocardial infarction. J Cell Mol Med 24:2717-2729 doi: 10.1111/jcmm.14953

10. Chang CW, Chiu CH, Lin MH, Wu HM, Yu TH, Wang PY, Kuo YY, Huang YY, Shiue CY, Huang WS, Yeh SH (2021) GMP-compliant fully automated radiosynthesis of [18F]FEPPA for PET/MRI imaging of regional brain TSPO expression. EJNMMI Res 11:26 doi: 10.1186/s13550-021-00768-9

11. Chen C, Kuo J, Wong A, Micevych P (2014) Estradiol modulates translocator protein (TSPO) and steroid acute regulatory protein (StAR) via protein kinase A (PKA) signaling in hypothalamic astrocytes. Endocrinology 155:2976-2985 doi: 10.1210/en.2013-1844

12. Chen Y, Ohmori K, Mizukawa M, Yoshida J, Zeng Y, Zhang L, Shinomiya K, Kosaka H, Kohno M (2007) Differential impact of atorvastatin vs pravastatin on progressive insulin resistance and left ventricular diastolic dysfunction in a rat model of type II diabetes. Circ J 71:144-152 doi: 10.1253/circj.71.144

13. Chung YW, Lagranha C, Chen Y, Sun J, Tong G, Hockman SC, Ahmad F, Esfahani SG, Bae DH, Polidovitch N, Wu J, Rhee DK, Lee BS, Gucek M, Daniels MP, Brantner CA, Backx PH, Murphy E, Manganiello VC (2015) Targeted disruption of PDE3B, but not PDE3A, protects murine heart from ischemia/reperfusion injury. Proc Natl Acad Sci USA 112:E2253-E2262 doi: 10.1073/pnas.1416230112

14. Desai R, East DA, Hardy L, Faccenda D, Rigon M, Crosby J, Alvarez MS, Singh A, Mainenti M, Hussey LK, Bentham R, Szabadkai G, Zappulli V, Dhoot GK, Romano LE, Xia D, Coppens I, Hamacher-Brady A, Chapple JP, Abeti R, Fleck RA, Vizcay-Barrena G, Smith K, Campanella M (2020) Mitochondria form contact sites with the nucleus to couple prosurvival retrograde response. Sci Adv 2020 6:eabc9955 doi: 10.1126/sciadv.abc9955

15. Egashira K, Ni W, Inoue S, Kataoka C, Kitamoto S, Koyanagi M, Takeshita A (2000) Pravastatin attenuates cardiovascular inflammatory and proliferative changes in a rat model of chronic inhibition of nitric oxide synthesis by its cholesterol-lowering independent actions. Hypertens Res 23:353-358 doi: 10.1291/hypres.23.353

16. Fan J, Campioli E, Midzak A, Culty M, Papadopoulos V (2015) Conditional steroidogenic cell-targeted deletion of TSPO unveils a crucial role in viability and hormone-dependent steroid formation. Proc Natl Acad Sci USA 112:7261-7266 doi: 10.1073/pnas.1502670112

17. Favre J, Gao J, Henry JP, Remy-Jouet I, Fourquaux I, Billon-Gales A, Thuillez C, Arnal JF, Lenfant F, Richard V (2010) Endothelial estrogen receptor {alpha} plays an essential

role in the coronary and myocardial protective effects of estradiol in ischemia/reperfusion. Arterioscler Thromb Vasc Biol 30:2562-2567 doi: 10.1161/ATVBAHA.110.213637

18. Fontaine D, Fontaine J, Dupont I, Dessy C, Piech A, Carpentier Y, Berkenboom G (2002) Chronic hydroxymethylglutaryl coenzyme a reductase inhibition and endothelial function of the normocholesterolemic rat: comparison with angiotensin-converting enzyme inhibition. J Cardiovasc Pharmacol 40:172-180 doi: 10.1097/00005344-200208000-00002

19. Galano M, Li Y, Li L, Sottas C, Papadopoulos V (2021) Role of Constitutive STAR in Leydig Cells. Int J Mol Sci 22:2021 doi: 10.3390/ijms22042021

20. Gatliff J, East D, Crosby J, Abeti R, Harvey R, Craigen W, Parker P, Campanella M (2014) TSPO interacts with VDAC1 and triggers a ROS-mediated inhibition of mitochondrial quality control. Autophagy 10:2279-2296 doi: 10.4161/15548627.2014.991665

21. Gatliff J, East DA, Singh A, Alvarez MS, Frison M, Matic I, Ferraina C, Sampson N, Turkheimer F, Campanella M (2017) A role for TSPO in mitochondrial Ca2+ homeostasis and redox stress signaling. Cell Death Dis 8:e2896 doi: 10.1038/cddis.2017.186

22. Gliozzi M, Scarano F, Musolino V, Carresi C, Scicchitano M, Ruga S, Zito MC, Nucera S, Bosco F, Maiuolo J, Macrì R, Guarnieri L, Mollace R, Coppoletta AR, Nicita C, Tavernese A, Palma E, Muscoli C, Mollace V (2020) Role of TSPO/VDAC1 Upregulation and Matrix Metalloproteinase-2 Localization in the Dysfunctional Myocardium of Hyperglycaemic Rats. Int J Mol Sci 21:7432 doi: 10.3390/ijms21207432

23. Gomez-Sanchez EP, Gomez-Sanchez CE (2021) 11β-hydroxysteroid dehydrogenases: A growing multi-tasking family. Mol Cell Endocrinol 526:111210 doi: 10.1016/j.mce.2021.111210

24. Griffiths EJ, Halestrap AP (1995) Mitochondrial non-specific pores remain closed during cardiac ischaemia, but open upon reperfusion. Biochem J 307:939-948 doi: 10.1042/bj3070093

25. Halestrap AP, Richardson AP (2015) The mitochondrial permeability transition: a current perspective on its identity and role in ischaemia/reperfusion injury. J Mol Cell Cardiol 78:129-141 doi: 10.1016/j.yjmcc.2014.08.018

26. Hans G, Wislet-Gendebien S, Lallemend F, Robe P, Rogister B, Belachew S, Nguyen L, Malgrange B, Moonen G, Rigo JM (2005) Peripheral benzodiazepine receptor (PBR) ligand cytotoxicity unrelated to PBR expression. Biochem Pharmacol 69:819-830 doi: 10.1016/j.bcp.2004.11.029

27. Hauet T, Yao ZX, Bose HS, Wall CT, Han Z, Li W, Hales DB, Miller WL, Culty M, Papadopoulos V (2005) Peripheral-type benzodiazepine receptor-mediated action of

925 steroidogenic acute regulatory protein on cholesterol entry into leydig cell mitochondria.
926 Mol Endocrinol 19:540-554 doi: 10.1210/me.2004-0307

927 28. Heusch G (2020) Myocardial ischaemia-reperfusion injury and cardioprotection in
928 perspective. Nat Rev Cardiol 17:773-789 doi: 10.1038/s41569-020-0403-y

929 29. Heusch G (2024) Myocardial ischemia/reperfusion: Translational pathophysiology of
930 ischemic heart disease. Med 5:10-31 doi: 10.1016/j.medj.2023.12.007

931 30. Huang Y, Walker KE, Hanley F, Narula J, Houser SR, Tulenko TN (2004) Cardiac systolic
932 and diastolic dysfunction after a cholesterol-rich diet. Circulation 109:97-102 doi:
933 10.1161/01.CIR.0000109213.10461.F6

934 31. Lecour S, Bøtker HE, Condorelli G, Davidson SM, Garcia-Dorado D, Engel FB, Ferdinandy
935 P, Heusch G, Madonna R, Ovize M, Ruiz-Meana M, Schulz R, Sluijter JP, Van Laake LW,
936 Yellon DM, Hausenloy DJ (2014) ESC working group cellular biology of the heart: position
937 paper: improving the preclinical assessment of novel cardioprotective therapies.
938 Cardiovasc Res 104:399-411 doi:10.1093/cvr/cvu225

939 32. Leducq N, Bono F, Sulpice T, Vin V, Janiak P, Fur GL, O'Connor SE, Herbert JM (2003)
940 Role of peripheral benzodiazepine receptors in mitochondrial, cellular, and cardiac
941 damage induced by oxidative stress and ischemia-reperfusion. J Pharmacol Exp Ther
942 306:828-837 doi: 10.1124/jpet.103.052068

943 33. Lee TM, Chou TF, Tsai CH (2003) Effects of pravastatin on cardiomyocyte hypertrophy
944 and ventricular vulnerability in normolipidemic rats after myocardial infarction. J Mol Cell
945 Cardiol 35:1449-1459 doi: 10.1016/j.yjmcc.2003.09.009

946 34. Liu D, Wang Z, Nicolas V, Lindner M, Mika D, Vandecasteele G, Fischmeister R, Brenner
947 C (2019) PDE2 regulates membrane potential, respiration and permeability transition of
948 rodent subsarcolemmal cardiac mitochondria. Mitochondrion 47:64-75 doi:
949 10.1016/j.mito.2019.05.002

950 35. Marín-Royo G, Ortega-Hernández A, Martínez-Martínez E, Jurado-López R, Luaces M,
951 Islas F, Gómez-Garre D, Delgado-Valero B, Lagunas E, Ramchandani B, García-Bouza
952 M, Nieto ML, Cachofeiro V (2019) The Impact of Cardiac Lipotoxicity on Cardiac Function
953 and Mirnas Signature in Obese and Non-Obese Rats with Myocardial Infarction. Sci Rep
954 9:444 doi: 10.1038/s41598-018-36914-y

955 36. McCommis KS, McGee AM, Laughlin MH, Bowles DK, Baines CP (2011)
956 Hypercholesterolemia increases mitochondrial oxidative stress and enhances the MPT
957 response in the porcine myocardium: beneficial effects of chronic exercise. Am J Physiol
958 Regul Integr Comp Physiol 301:R1250-1258 doi: 10.1152/ajpregu.00841.2010

959 37. Miller WL (2013) Steroid hormone synthesis in mitochondria. Mol Cell Endocrinol 379:62-
960 73 doi: 10.1016/j.mce.2013.04.014

961 38. Morin D, Long R, Panel M, Laure L, Taranu A, Gueguen C, Pons S, Leoni V, Caccia C,
962 Vatner SF, Vatner DE, Qiu H, Depre C, Berdeaux A, Ghaleh B (2019) Hsp22
963 overexpression induces myocardial hypertrophy, senescence and reduced life span
964 through enhanced oxidative stress. Free Radic Biol Med 137:194-200 doi:
965 10.1016/j.freeradbiomed.2019.04.035

966 39. Morin D, Musman J, Pons S, Berdeaux A, Ghaleh B (2016) Mitochondrial translocator
967 protein (TSPO): From physiology to cardioprotection. Biochem Pharmacol 105:1-13 doi:
968 10.1016/j.bcp.2015.12.003

969 40. Morohaku K, Pelton SH, Daugherty DJ, Butler WR, Deng W, Selvaraj V (2014)
970 Translocator protein/peripheral benzodiazepine receptor is not required for steroid
971 hormone biosynthesis. Endocrinology 155:89-97 doi: 10.1210/en.2013-1556

972 41. Musman J, Paradis S, Panel M, Pons S, Barau C, Caccia C, Leoni V, Ghaleh B, Morin D
973 (2017) A TSPO ligand prevents mitochondrial sterol accumulation and dysfunction during
974 myocardial ischemia-reperfusion in hypercholesterolemic rats. Biochem Pharmacol
975 142:87-95 doi: 10.1016/j.bcp.2017.06.125

976 42. Musman J, Pons S, Barau C, Caccia C, Leoni V, Berdeaux A, Ghaleh B, Morin D (2016)
977 Regular treadmill exercise inhibits mitochondrial accumulation of cholesterol and
978 oxysterols during myocardial ischemia-reperfusion in wild-type and ob/ob mice. Free
979 Radic Biol Med 101:317-324 doi: 10.1016/j.freeradbiomed.2016.10.496

980 43. Neil A, Cooper J, Betteridge J, Capps N, McDowell I, Durrington P, Seed M, Humphries
981 SE (2008) Reductions in all-cause, cancer, and coronary mortality in statin-treated
982 patients with heterozygous familial hypercholesterolaemia: a prospective registry study.
983 Eur Heart J 29:2625-2633 doi: 10.1093/eurheartj/ehn422

984 44. Nutma E, Ceyzériat K, Amor S, Tsartsalis S, Millet P, Owen DR, Papadopoulos V, Tournier
985 BB (2021) Cellular sources of TSPO expression in healthy and diseased brain. Eur J Nucl
986 Med Mol Imaging 49:146-163 doi: 10.1007/s00259-020-05166-2

987 45. Obame FN, Zini R, Souktani R, Berdeaux A, Morin D (2007) Peripheral benzodiazepine
988 receptor-induced myocardial protection is mediated by inhibition of mitochondrial
989 membrane permeabilization. J Pharmacol Exp Ther 323:336-345 doi:
990 10.1124/jpet.107.124255

46. Onody A, Csonka C, Giricz Z, Ferdinandy P (2003) Hyperlipidemia induced by a cholesterol-rich diet leads to enhanced peroxynitrite formation in rat hearts. Cardiovasc Res 58:663-670 doi: 10.1016/s0008-6363(03)00330-4

47. Osipov RM, Bianchi C, Feng J, Clements RT, Liu Y, Robich MP, Glazer HP, Sodha NR, Sellke FW (2009) Effect of hypercholesterolemia on myocardial necrosis and apoptosis in the setting of ischemia-reperfusion. Circulation 120:S22-30 doi: 10.1161/CIRCULATIONAHA.108.842724

48. Owen DR, Fan J, Campioli E, Venugopal S, Midzak A, Daly E, Harlay A, Issop L, Libri V, Kalogiannopoulou D, Oliver E, Gallego-Colon E, Colasanti A, Huson L, Rabiner EA, Suppiah P, Essagian C, Matthews PM, Papadopoulos V (2017) TSPO mutations in rats and a human polymorphism impair the rate of steroid synthesis. Biochem J 474:3985-3999 doi: 10.1042/BCJ20170648

49. Papadopoulos V (2014) On the role of the translocator protein (18-kDa) TSPO in steroid hormone biosynthesis. Endocrinology 155:15-20 doi: 10.1210/en.2013-2033

50. Papadopoulos V, Aghazadeh Y, Fan F, Campioli E, Zirkin B, Midzak A (2015) Translocator protein-mediated pharmacology of cholesterol transport and steroidogenesis. Mol Cell Endocrinol 408:90-98 doi: 10.1016/j.mce.2015.03.014

51. Paradis S, Leoni V, Caccia C, Berdeaux A, Morin D (2013) Cardioprotection by the TSPO ligand 4'-chlorodiazepam is associated with inhibition of mitochondrial accumulation of cholesterol at reperfusion. Cardiovasc Res 98:420-427 doi: 10.1093/cvr/cvt079

52. Penumathsa SV, Thirunavukkarasu M, Koneru S, Juhasz B, Zhan L, Pant R, Menon VP, Otani H, Maulik N (2007) Statin and resveratrol in combination induces cardioprotection against myocardial infarction in hypercholesterolemic rat. J Mol Cell Cardiol 42:508-516 doi: 10.1016/j.yjmcc.2006.10.018

53. Pitasi CL, Liu J, Gausserès B, Pommier G, Delangre E, Armanet M, Cattan P, Mégarbane B, Hanak AS, Maouche K, Bailbé D, Portha B, Movassat J (2020) Implication of glycogen synthase kinase 3 in diabetes-associated islet inflammation. J Endocrinol 244:133-148 doi: 10.1530/JOE-19-0239

54. Raal FJ, Pilcher GJ, Panz VR, van Deventer HE, Brice BC, Blom DJ, Marais AD (2011) Reduction in mortality in subjects with homozygous familial hypercholesterolemia associated with advances in lipid-lowering therapy. Circulation 124:2202-2207 doi: 10.1161/CIRCULATIONAHA.111.042523

55. Reed GW, Rossi JE, Cannon CP (2017) Acute myocardial infarction. Lancet 389:197-210 doi:10.1016/S0140-6736(16)30677-8

56. Rojas S, Martín A, Arranz MJ, Pareto D, Purroy J, Verdaguer E, Llop J, Gómez V, Gispert JD, Millán O, Chamorro A, Planas AM (2007) Imaging brain inflammation with [(11)C]PK11195 by PET and induction of the peripheral-type benzodiazepine receptor after transient focal ischemia in rats. J Cereb Blood Flow Metab 27:1975-1986 doi: 10.1038/sj.jcbfm.9600500

57. Rone MB, Fan J, Papadopoulos V (2009) Cholesterol transport in steroid biosynthesis: role of protein-protein interactions and implications in disease states. Biochim Biophys Acta 1791:646-658 doi: 10.1016/j.bbalip.2009.03.001

58. Schaller S, Paradis S, Ngoh GA, Assaly R, Buisson B, Drouot C, Ostuni MA, Lacapere JJ, Bassissi F, Bordet T, Berdeaux A, Jones SP, Morin D, Pruss RM (2010) TRO40303, a new cardioprotective compound, inhibits mitochondrial permeability transition. J Pharmacol Exp Ther 333:696-706 doi: 10.1124/jpet.110.167486

59. Šileikytė J, Blachly-Dyson E, Sewell R, Carpi A, Menabò R, Di Lisa F, Ricchelli F, Bernardi P, Forte M (2014) Regulation of the mitochondrial permeability transition pore by the outer membrane does not involve the peripheral benzodiazepine receptor (Translocator Protein of 18 kDa (TSPO)). J Biol Chem 1289:13769-13781 doi: 10.1074/jbc.M114.549634

60. Sniderman AD, Tsimikas S, Fazio S (2014) The severe hypercholesterolemia phenotype: clinical diagnosis, management, and emerging therapies. J Am Coll Cardiol 63:1935-1947 doi:10.1016/j.jacc.2014.01.060

61. Tian H, Zhao X, Zhang Y, Xia Z (2023) Abnormalities of glucose and lipid metabolism in myocardial ischemia-reperfusion injury. Biomed Pharmacother 163:114827 doi: 10.1016/j.biopha.2023.114827

62. Tu LN, Morohaku K, Manna PR, Pelton SH, Butler WR, Stocco DM, Selvaraj V (2014) Peripheral benzodiazepine receptor/translocator protein global knock-out mice are viable with no effects on steroid hormone biosynthesis. J Biol Chem 289:27444-27454 doi: 10.1074/jbc.M114.578286

63. Tu LN, Zhao AH, Stocco DM, Selvaraj V (2015) PK11195 effect on steroidogenesis is not mediated through the translocator protein (TSPO). Endocrinology 156:1033-1039 doi: 10.1210/en.2014-1707

64. Varga ZV, Kupai K, Szűcs G, Gáspár R, Pálóczi J, Faragó N, Zvara A, Puskás LG, Rázga Z, Tiszlavicz L, Bencsik P, Görbe A, Csonka C, Ferdinandy P, Csont T (2013) MicroRNA-25-dependent up-regulation of NADPH oxidase 4 (NOX4) mediates hypercholesterolemia-induced oxidative/nitrative stress and subsequent dysfunction in the heart. J Mol Cell Cardiol 62:111-121 doi: 10.1016/j.yjmcc.2013.05.009

65. Vejux A, Ghzaiel I, Nury T, Schneider V, Charrière K, Sghaier R, Zarrouk A, Leoni V, Moreau T, Lizard G (2021) Oxysterols and multiple sclerosis: Physiopathology, evolutive biomarkers and therapeutic strategy. J Steroid Biochem Mol Biol 210:105870 doi: 10.1016/j.jsbmb.2021.105870

66. Walker BR, Yau JL, Brett LP, Seckl JR, Monder C, Williams BC, Edwards CR (1991) 11 beta-hydroxysteroid dehydrogenase in vascular smooth muscle and heart: implications for cardiovascular responses to glucocorticoids. Endocrinology 129:3305-3312 doi: 10.1210/endo-129-6-3305

67. Wong HS, Dighe PA, Mezera V, Monternier PA, Brand MD (2017) Production of superoxide and hydrogen peroxide from specific mitochondrial sites under different bioenergetic conditions. J Biol Chem 292:16804-16809 doi: 10.1074/jbc.R117.789271

68. Young MJ, Clyne CD, Cole TJ, Funder JW (2001) Cardiac steroidogenesis in the normal and failing heart. J Clin Endocrinol Metab 86:5121-5126 doi: 10.1210/jcem.86.11.7925

Figure Legends

Fig. 1. *Tspo* deletion in Spague Dawley rats. (**a**): Agarose gel image of the typical PCR products used for genotyping screening of rat with *Tspo* locus modification (*Tspo*$^{+/+}$, 362 bp; *Tspo*$^{+/-}$, two bands 362 and 273 bp; *Tspo*$^{-/-}$, 273 bp) and primers used for genotyping. (**b**): Representative immunohistochemical images of TSPO in myocardium showing the lack of TSPO *in Tspo*$^{-/-}$ rats of 2-month-old. Magnification: 400x, scale-bar: 50 µm. (**c**): Immunoblot analysis of cardiac mitochondria extracted from *Tspo*$^{+/+}$ and *Tspo*$^{-/-}$ rats. Voltage-dependent anion channel (VDAC) was used as a loading control. Each value represents the mean ± SEM of 3 independent mitochondrial preparations. Statistical analysis was done using an unpaired two-tailed t-test

Fig. 2. Effects of pravastatin (P) treatment on the level of cholesterol and oxysterols in cardiac mitochondria (**a**, **d**), cytosols (**b**, **e**) and plasma (**c**) of rats subjected or not to cardiac ischemia-reperfusion (I/R). 7α-hydroxycholesterol (7αOHC); 7β-hydroxycholesterol (7βOHC); 7-ketocholesterol (7KC); cholesterol-5α,6α-epoxide (αEpoxiC); cholesterol-5β,6β-epoxide (βEpoxiC). Each value is the mean of 9-15 independent experiments. All the figures were analyzed by a two-way ANOVA followed by a Tukey's multi-comparison test

Fig. 3. Effect of ischemia-reperfusion (I/R) on cardiac CYP11A, CYP27A1, TSPO and STAR expression. (**a**)**:** I/R does not alter protein level mitochondrial protein levels and mRNA left ventricle expression of CYP11A1 and CYP27A. COX-IV was used as a loading control. (**b**):

Expression of CYP11A1 and CYP27A1 in cardiac mitochondria compared to their respective control organs (testis and liver), respectively (n=3, independent mitochondrial preparations). (**c**): Representative experiment measuring CYP11A1 enzymatic activity in testis, sham and I/R cardiac mitochondria (left). Quantification of CYP11A1 enzymatic activity (right). Each value is the mean ± SEM of 4-6 independent mitochondrial preparations. Statistical analysis: one way ANOVA followed by a Tukey's multi-comparison test. (**d**): I/R does not alter mitochondrial level of TSPO. (**e**): I/R decreases cytosolic level of STAR 37-kDa. (**f**): I/R increases mitochondria level of STAR 30-kDa. (**g**): I/R does not alter *Tspo* but decreases *Star* mRNA expression in the myocardium. Each value is the mean ± SEM of at least 3 independent preparations (**c-g**). COX-IV (**d** and **e**) and actin (**f**) were used as a loading control. Statistical analyses were done using an unpaired two-tailed t-test (**c-f)** or a two-way ANOVA followed by a Sidak's multi-comparison test (**g**). ns: non-significant

Fig. 4. Effect of pravastatin and 4'-chlorodiazepam treatment on mitochondrial STAR level after cardiac ischemia-reperfusion (I/R). (**a**): Effect of pravastatin (P). Statistical analysis was done by a two-way ANOVA analysis followed by a Tukey's multi-comparison test. (**b**): Effect of 4'-chlorodiazepam (CDZ). Statistical analysis was done by a one-way ANOVA analysis followed by a Tukey's multi-comparison test. COX-IV was used as a loading control. Each value is the mean ± SEM of at least 3 mitochondrial independent preparations

Fig. 5. Effects of Tspo deletion on cholesterol (**a**) and oxysterols (**b-g**) in cardiac mitochondria in rats subjected or not to cardiac ischemia-reperfusion (I/R). Each value is the mean ± SEM of 6-7 independent experiments. All the panels were analyzed by a two-way ANOVA followed by a Tukey's multi-comparison test. White bars: $Tspo^{+/+}$ rats. Grey bars: $Tspo^{-/-}$ rats. ns: non-significant

Fig. 6. Effects of *Tspo* deletion on mitochondrial oxidative stress. (**a**)***:*** *Left:* time-dependent mitochondrial superoxide production in cardiomyocytes isolated from $Tspo^{+/+}$ and $Tspo^{-/-}$ rats. Each point is the mean of 9-10 independent cardiomyocyte preparations, each preparation including 20-30 cells. Statistical comparison was done by two-way ANOVA analysis. *Right:* representative images obtained at t=0 and 60 min. Scale bar: 200 µm. (**b**): Lipid peroxidation as indicated by 4-hydroxynonenal levels in cardiac mitochondria (mito) and cytosols (cyto) isolated from $Tspo^{+/+}$ and $Tspo^{-/-}$ rats. Each value is the mean ± SEM of 6 independent preparations. Statistical analysis was done using an unpaired two-tailed t-test. (**c**): Superoxide anion generation was assessed in isolated myocardial mitochondria by measuring the rate of hydrogen peroxide production. Superoxide anion production was induced by pyruvate/malate

(P/M; 5/5 mM) or succinate (Succ;5 mM) in the presence or absence of 1 µM rotenone (Rot) and 1 µM antimycin A (AA) and was determined fluorometrically by the oxidation of Amplex red to resorufin. Each value is the mean ± SEM of 5-6 independent mitochondrial preparations. (**d**): Western blot analysis and quantification of SOD2 and VDAC in *Tspo*$^{+/+}$ and *Tspo*$^{-/-}$ cardiac mitochondria. Each value is the mean ± SEM of 4-5 independent mitochondrial preparations. COX-IV was used as a loading control. A.U.: arbitrary units

Fig. 7. Effect of *Tspo* deletion on mitochondrial function in rats subjected or not to cardiac ischemia-reperfusion (I/R) and on infarct size. Mitochondrial yield (**a**), oxygen consumption (**b**,**c**) and calcium retention capacity (**d**) in cardiac mitochondria isolated from *Tspo*$^{+/+}$ and *Tspo*$^{-/-}$ rats subjected to I/R and treated or not with 4'-chlorodiazepam (CDZ). Each value is the mean ± SEM of at least 6 independent experiments. All the figures were analyzed by a two-way ANOVA followed by a Tukey's multi-comparison test. (**e**): Infarct size (expressed as percentage of the area at risk) measured in *Tspo*$^{+/+}$ and *Tspo*$^{-/-}$ rats subjected to 30 min of coronary artery occlusion and 24 h of reperfusion. The areas at risk (insert) were similar in both groups.

Fig. 8. Deletion of *Tspo* inhibits the effect of 4'-chlorodiazepam (CDZ) on mitochondrial STAR and cholesterol accumulation after ischemia-reperfusion (I/R) but does not affect cytosolic STAR level. (**a**) and (**b**): effect of CDZ on mitochondrial STAR and cholesterol accumulation in *Tspo*$^{+/+}$ rats. (**c**) and (**d**): effect of CDZ on mitochondrial STAR and cholesterol accumulation in *Tspo*$^{-/-}$ rats. (**e**): effect of I/R on cytosolic STAR 37-kDa level in *Tspo*$^{+/+}$ rats. (**f**): effect of CDZ treatment on cytosolic STAR 37-kDa level after I/R in *Tspo*$^{+/+}$ rats. (**g**): effect of I/R on cytosolic STAR 37-kDa level in *Tspo*$^{-/-}$ rats. (**h**): effect of CDZ treatment on cytosolic STAR 37-kDa level after I/R in *Tspo*$^{-/-}$ rats. COX-IV and GAPDH was used as a loading control. Each value is the mean ± SEM of 3-5, 3-6 and 6-7 independent preparations for mitochondrial western blot, cytosolic western blot and cholesterol dosage, respectively. Statistical analyses were done by an unpaired two-tailed t-test (**a, c, e-h**) and a two-way ANOVA analysis followed by a Tukey's multi-comparison test (**b** and **d**). ns: non-significant

Table 1 Effects of pravastatin treatment on respiration and calcium retention capacity of cardiac mitochondria from Wistar rats subjected to 30 min ischemia and 15 min reperfusion

	Sham (n=7)	**I/R** (n=10)	**I/R+P** (n=10)
Respiration			
Substrate-dependent respiration	36.3±2.24	43.6±3.59	42.1±3.4
ADP-stimulated respiration	234±8	131±11§	188±11‡
Respiratory control ratio	6.66±0.31	3.20±0.39§	4.75±0.5*
Calcium retention capacity	139±11	53±7§	81±7†

Respiration is expressed as nmoL/min/mg protein and calcium retention capacity in nmoL/mg protein. I/R: ischemia-reperfusion. P: pravastatin.

Each value is the mean ± SEM of 7-10 mitochondrial independent preparations. Data were analyzed by a one-way ANOVA followed by a Tukey's multi-comparison test. *p=0.0348, †p=0.0419 and ‡p=0.0017 *vs* respective I/R.

§p< 0.0001 *vs* respective Sham.

Table 2 Cardiac cytosolic concentrations of sterols in *Tspo*$^{+/+}$ and *Tspo*$^{-/-}$ rats

Sterols	***Tspo*$^{+/+}$**	***Tspo*$^{-/-}$**
Cholesterol (nmol/mg prot)	2.69 ± 0.08	2.60 ± 0.11
7α-hydroxycholesterol (pmol/mg prot)	1.28 ± 0.05	1.30 ± 0.04
7β-hydroxycholesterol (pmol/mg prot)	1.29 ± 0.04	1.31 ± 0.01
7-ketocholesterol (pmol/mg prot)	6.30 ± 0.19	6.31 ± 0.29
cholesterol-5α,6α-epoxide (pmol/mg prot)	1.96 ± 0.15	4.76 ± 0.60‡
cholesterol-5β,6β-epoxide (pmol/mg prot)	0.97 ± 0.04	0.77 ± 0.03†
25-hydroxycholesterol (pmol/mg prot)	3.58 ± 0.14	4.11 ± 0.18*

Each value is the mean ± SEM of 6 independent preparations. Data were analyzed by an unpaired two-tailed t-test. *p=0.042, †p=0.0025 and ‡p=0.001 vs respective *Tspo*$^{+/+}$

a

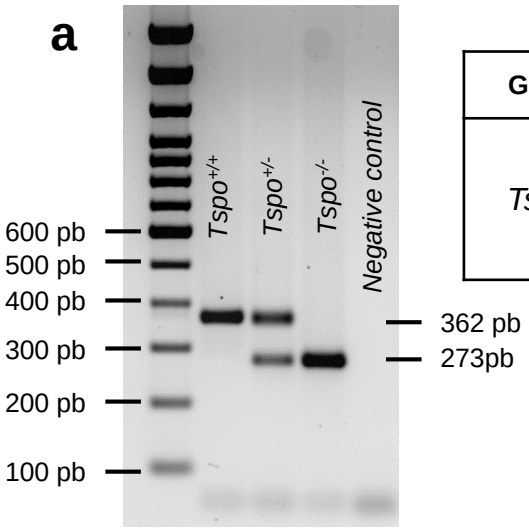

Gene	Primer name (reference)	Sequence (5' > 3')	Molecular weight	Melting temperature
Tspo	R5CKOZFN-R (6430489)	ACT-CCT-AAA-GGG-GTT-GCA-GG	6182,1 g/mol	62°C
	R5CKOZFN-F (6430488)	AGA-GCA-TAC-TCT-TGC-CGT-CG	6093,0 g/mol	62°C

b

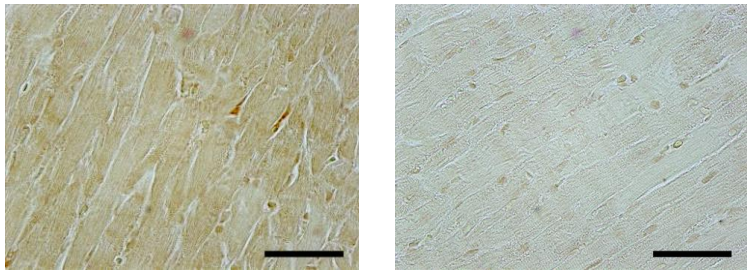

Tspo$^{+/+}$ *Tspo*$^{-/-}$

c

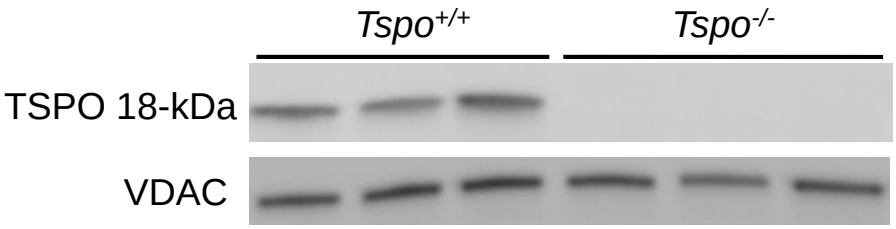

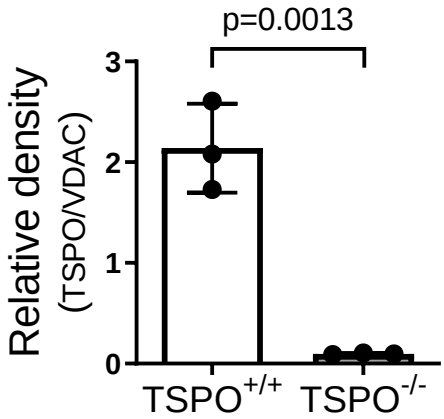

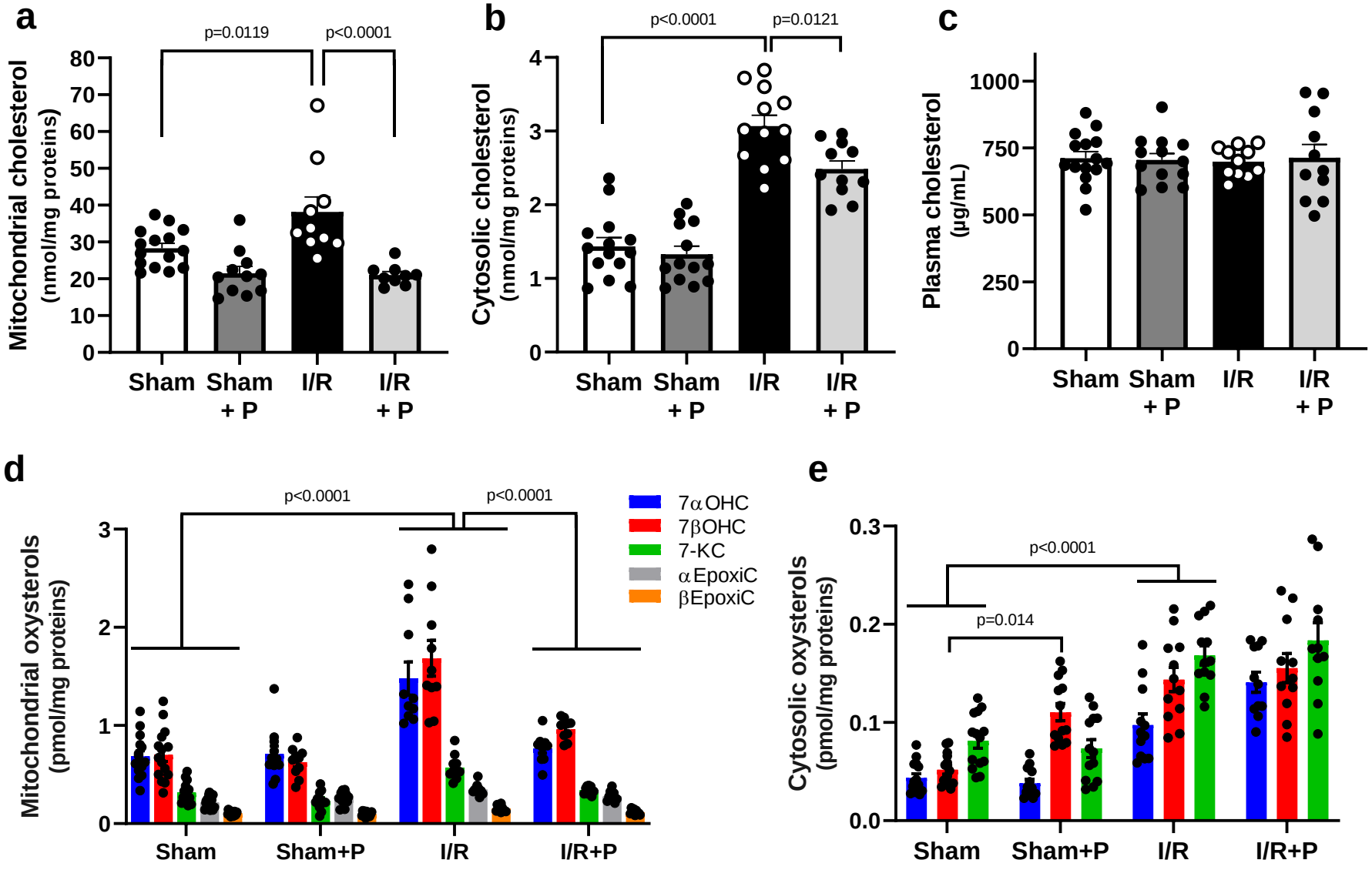
a
p=0.0119
p<0.0001
Mitochondrial cholesterol
(nmol/mg proteins)
80
70
60
50
40
30
20
10
0
Sham
Sham + P
I/R
I/R + P
b
p<0.0001
p=0.0121
Cytosolic cholesterol
(nmol/mg proteins)
4
3
2
1
0
Sham
Sham + P
I/R
I/R + P
c
Plasma cholesterol
(µg/mL)
1000
750
500
250
0
Sham
Sham + P
I/R
I/R + P
d
p<0.0001
p<0.0001
7αOHC
7βOHC
7-KC
αEpoxiC
βEpoxiC
Mitochondrial oxysterols
(pmol/mg proteins)
3
2
1
0
Sham
Sham+P
I/R
I/R+P
e
p<0.0001
p=0.014
Cytosolic oxysterols
(pmol/mg proteins)
0.3
0.2
0.1
0.0
Sham
Sham+P
I/R
I/R+P

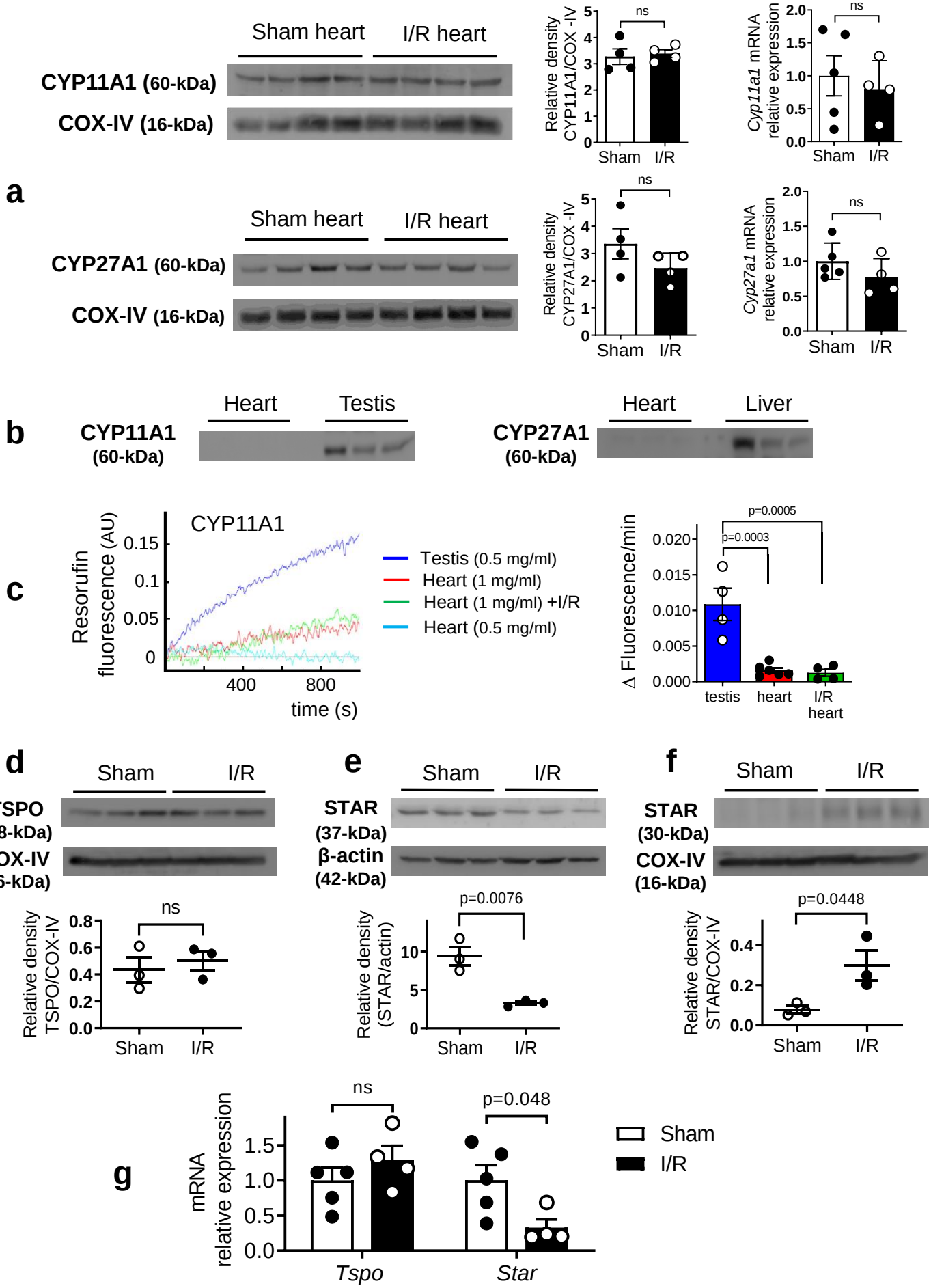
a
Sham heart
I/R heart
CYP11A1 (60-kDa)
COX-IV (16-kDa)
Relative density CYP11A1/COX -IV
ns
Sham
I/R
Cyp11a1 mRNA relative expression
CYP27A1 (60-kDa)
CYP27A1/COX -IV
Cyp27a1 mRNA relative expression
b
Heart
Testis
Liver
c
CYP11A1
Resorufin fluorescence (AU)
time (s)
Testis (0.5 mg/ml)
Heart (1 mg/ml)
Heart (1 mg/ml) +I/R
Heart (0.5 mg/ml)
Δ Fluorescence/min
p=0.0005
p=0.0003
testis
heart
I/R heart
d
TSPO (18-kDa)
COX-IV (16-kDa)
Relative density TSPO/COX-IV
e
STAR (37-kDa)
β-actin (42-kDa)
p=0.0076
Relative density (STAR/actin)
f
STAR (30-kDa)
p=0.0448
Relative density STAR/COX-IV
g
mRNA relative expression
p=0.048
Tspo
Star

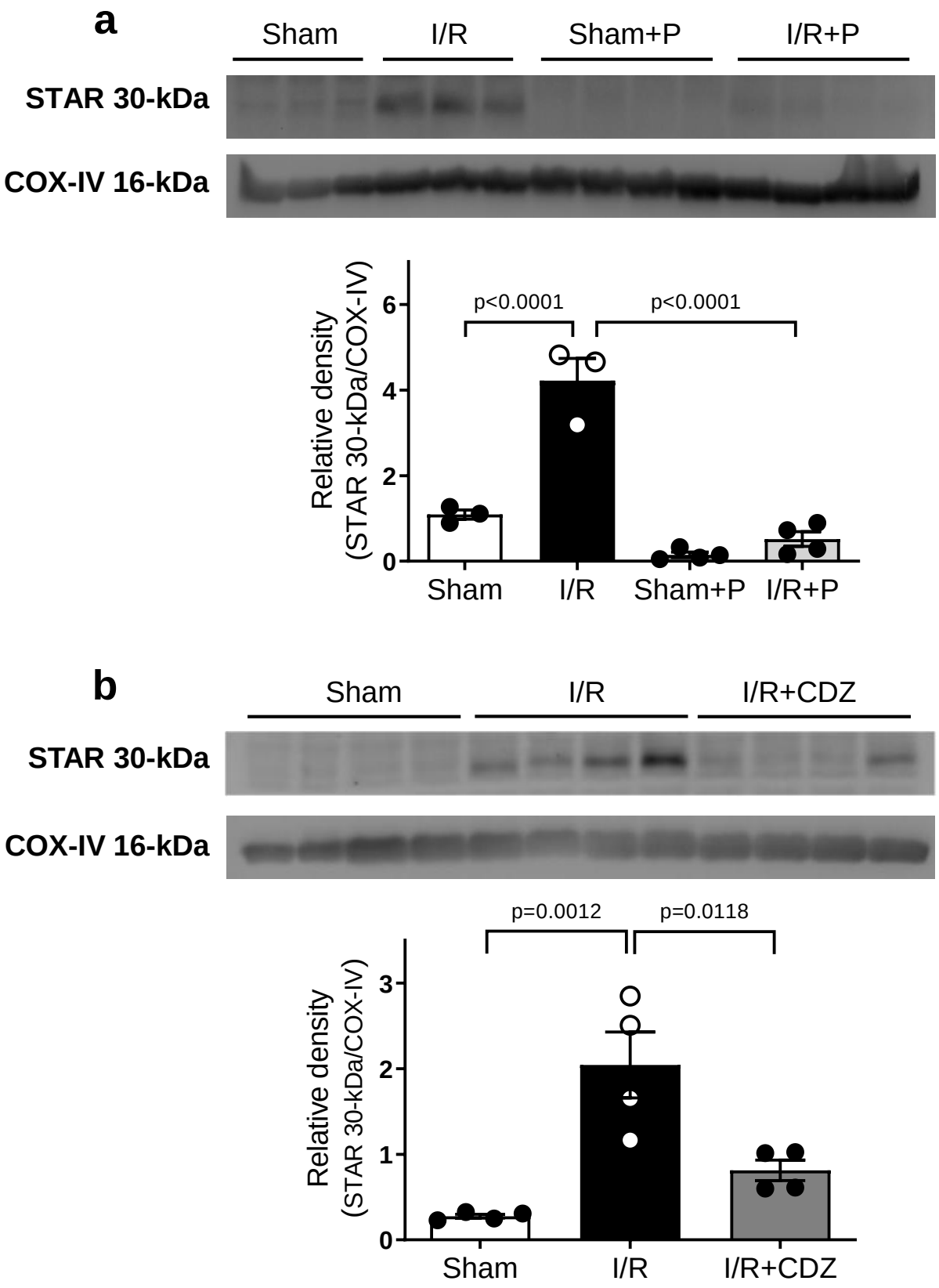
a
Sham
I/R
Sham+P
I/R+P
STAR 30-kDa
COX-IV 16-kDa
Relative density
(STAR 30-kDa/COX-IV)
p<0.0001
p<0.0001
0
2
4
6
Sham
I/R
Sham+P
I/R+P
b
Sham
I/R
I/R+CDZ
STAR 30-kDa
COX-IV 16-kDa
Relative density
(STAR 30-kDa/COX-IV)
p=0.0012
p=0.0118
0
1
2
3
Sham
I/R
I/R+CDZ

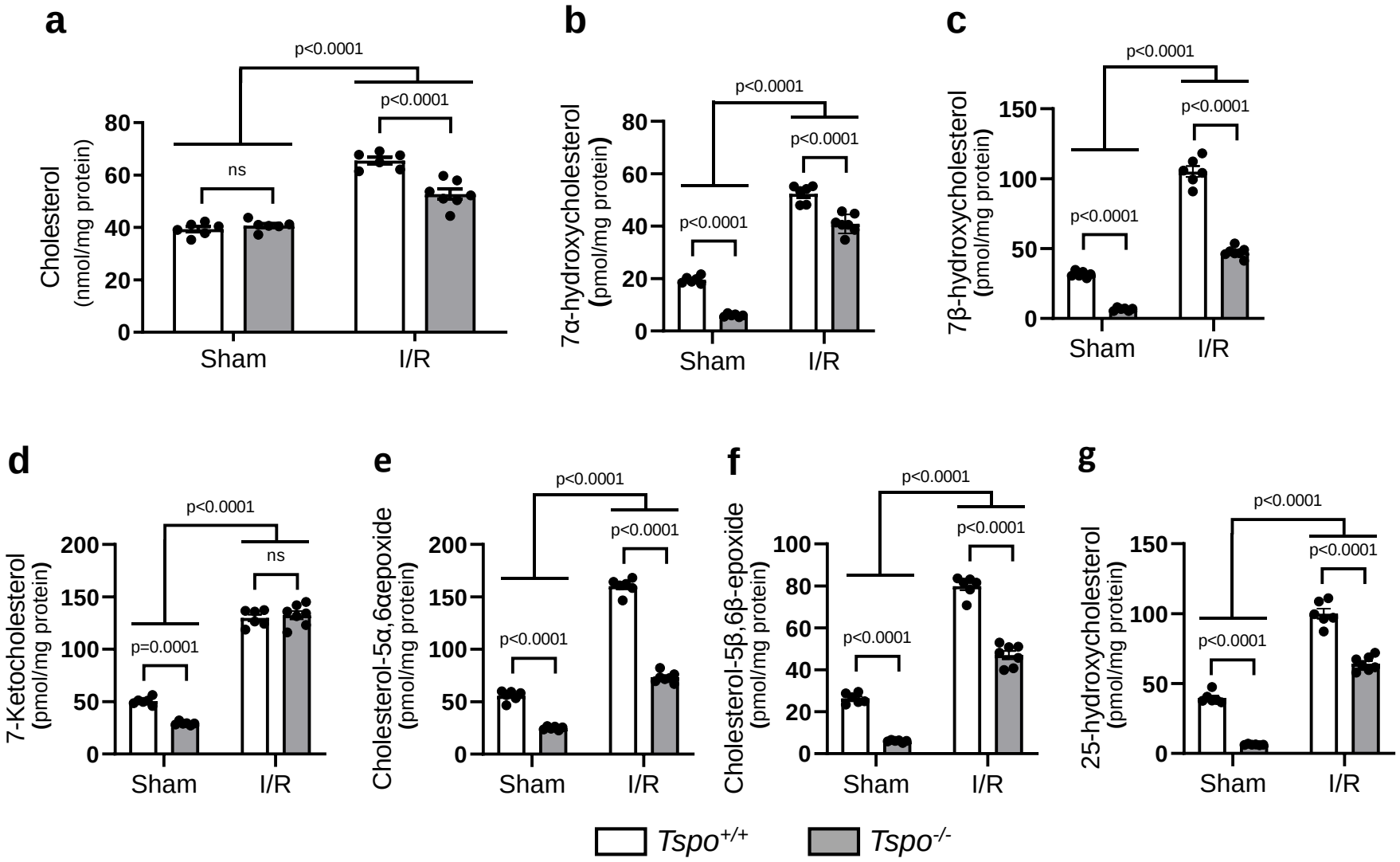
a
Cholesterol
(nmol/mg protein)
p<0.0001
p<0.0001
ns
80
60
40
20
0
Sham
I/R
b
7α-hydroxycholesterol
(pmol/mg protein)
p<0.0001
p<0.0001
p<0.0001
c
7β-hydroxycholesterol
(pmol/mg protein)
p<0.0001
p<0.0001
p<0.0001
150
100
50
d
7-Ketocholesterol
(pmol/mg protein)
p<0.0001
ns
p=0.0001
200
150
100
e
Cholesterol-5α,6αepoxide
(pmol/mg protein)
p<0.0001
p<0.0001
p<0.0001
f
Cholesterol-5β,6β-epoxide
(pmol/mg protein)
p<0.0001
p<0.0001
p<0.0001
g
25-hydroxycholesterol
(pmol/mg protein)
p<0.0001
p<0.0001
p<0.0001
Tspo+/+
Tspo-/-

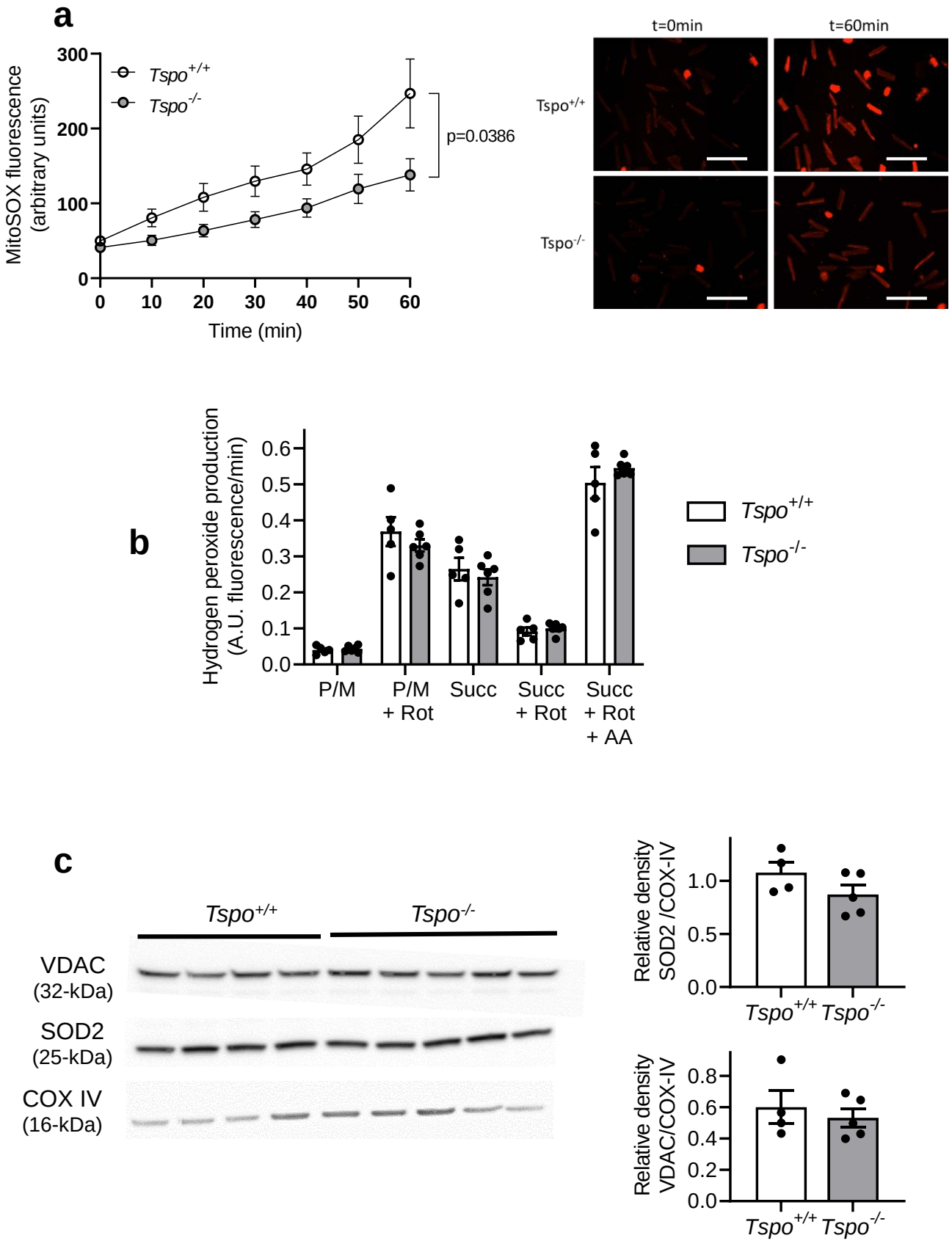
a
MitoSOX fluorescence (arbitrary units)
Tspo+/+
Tspo-/-
p=0.0386
Time (min)
t=0min
t=60min
Tspo+/+
Tspo-/-
b
Hydrogen peroxide production (A.U. fluorescence/min)
P/M
P/M + Rot
Succ
Succ + Rot
Succ + Rot + AA
Tspo+/+
Tspo-/-
c
Tspo+/+
Tspo-/-
VDAC (32-kDa)
SOD2 (25-kDa)
COX IV (16-kDa)
Relative density SOD2 /COX-IV
Relative density VDAC/COX-IV

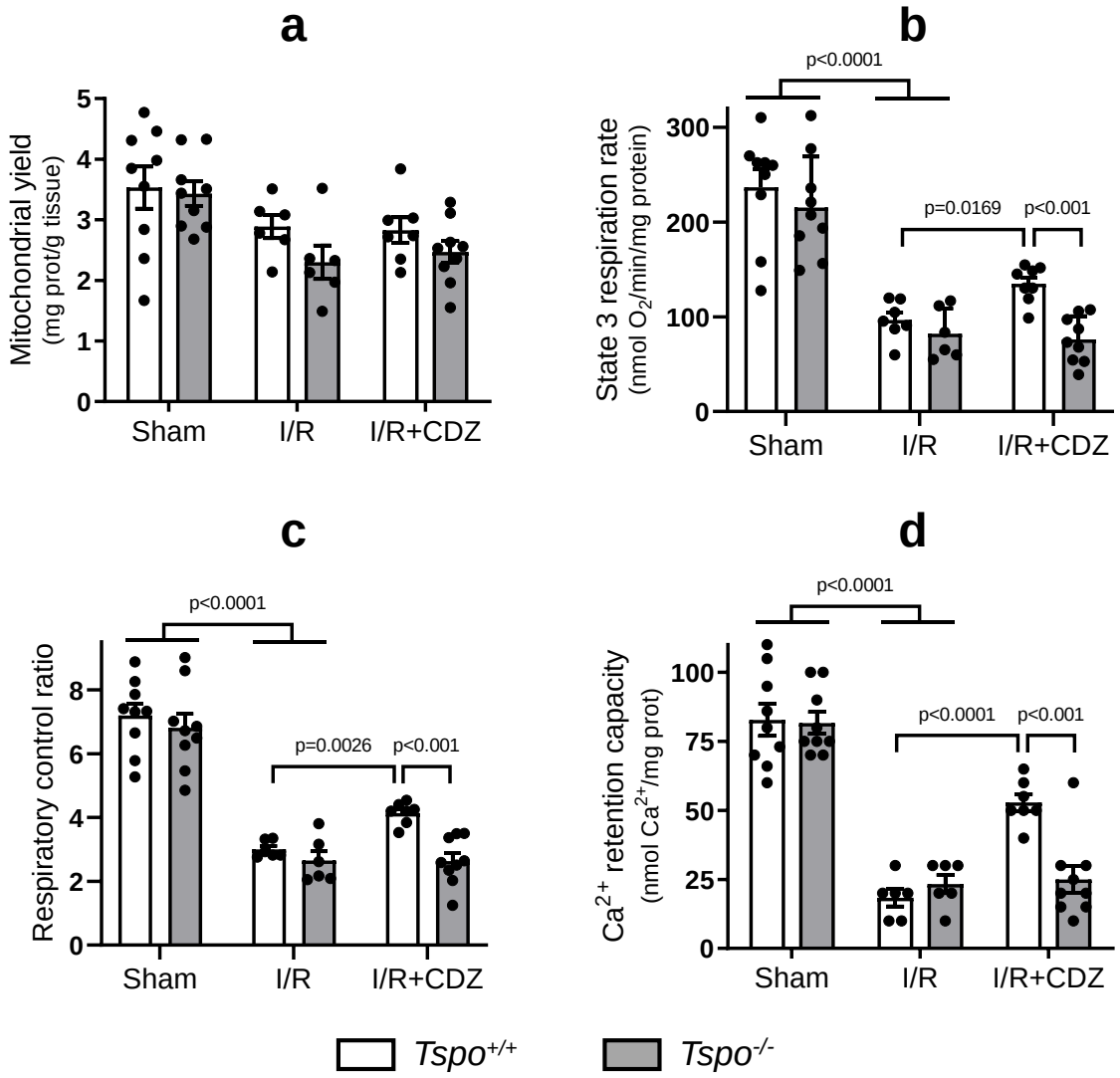
a
Mitochondrial yield
(mg prot/g tissue)
0
1
2
3
4
5
Sham
I/R
I/R+CDZ
b
State 3 respiration rate
(nmol O2/min/mg protein)
0
100
200
300
p<0.0001
p=0.0169
p<0.001
Sham
I/R
I/R+CDZ
c
Respiratory control ratio
0
2
4
6
8
p<0.0001
p=0.0026
p<0.001
Sham
I/R
I/R+CDZ
d
Ca2+ retention capacity
(nmol Ca2+/mg prot)
0
25
50
75
100
p<0.0001
p<0.0001
p<0.001
Sham
I/R
I/R+CDZ
Tspo+/+
Tspo-/-

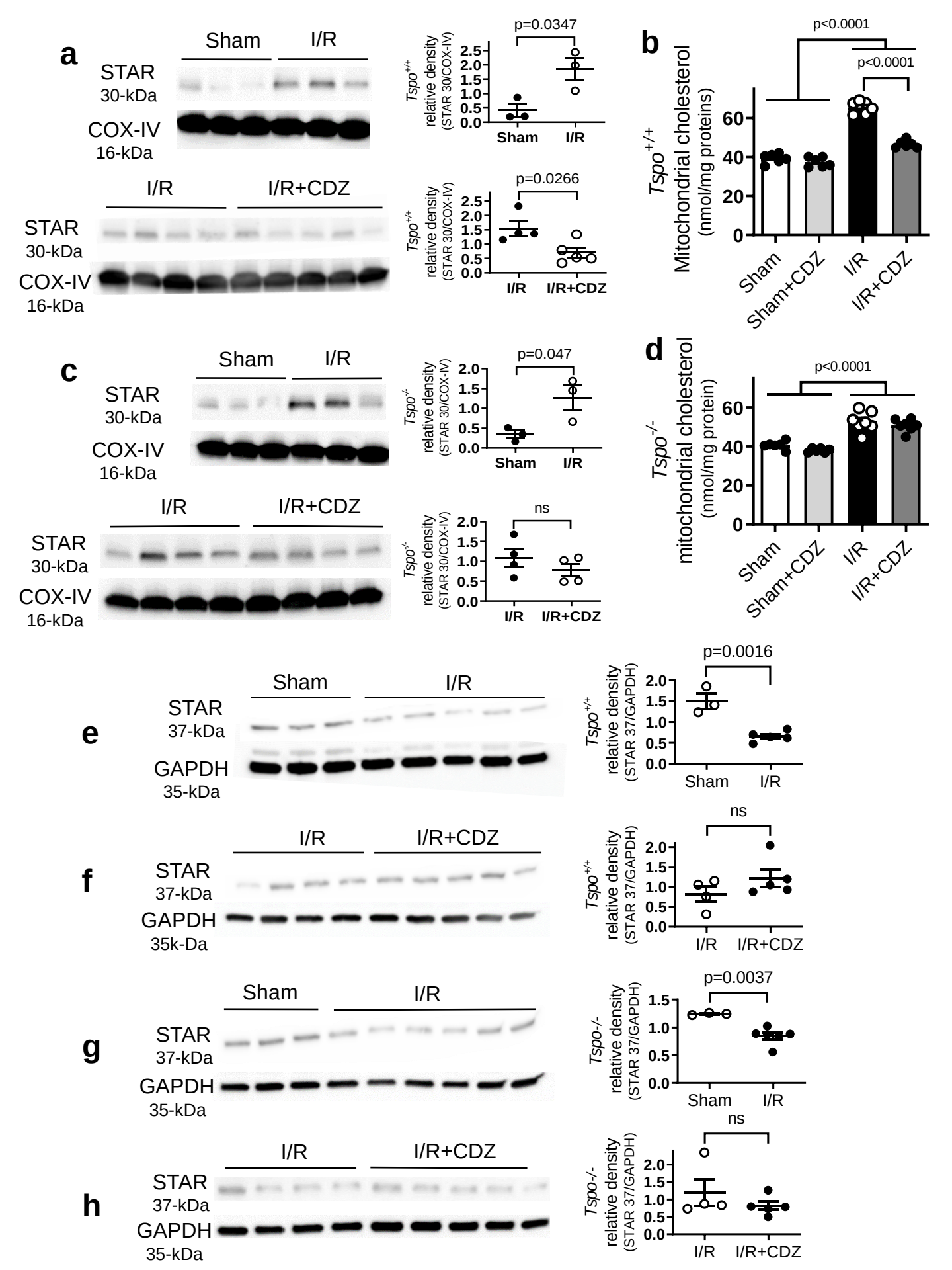
a
Sham
I/R
STAR
30-kDa
COX-IV
16-kDa
p=0.0347
Tspo+/+
relative density
(STAR 30/COX-IV)
Sham
I/R
I/R
I/R+CDZ
p=0.0266
I/R
I/R+CDZ
b
p<0.0001
p<0.0001
Tspo+/+
Mitochondrial cholesterol
(nmol/mg proteins)
Sham
Sham+CDZ
I/R
I/R+CDZ
c
p=0.047
Tspo-/-
ns
d
p<0.0001
Tspo-/-
mitochondrial cholesterol
(nmol/mg protein)
e
STAR
37-kDa
GAPDH
35-kDa
p=0.0016
Tspo+/+
relative density
(STAR 37/GAPDH)
f
35k-Da
ns
g
p=0.0037
Tspo-/-
h
ns

Journal: Basic Research in Cardiology

Identification of a mechanism promoting mitochondrial sterol accumulation during myocardial ischemia-reperfusion: role of TSPO and STAR

Juliette Bréhat[1], Shirin Leick[1], Julien Musman[1], Jin Bo Su[1], Nicolas Eychenne[2], Frank Giton[3], Michael Rivard[4], Louis-Antoine Barel[4], Chiara Tropeano[5], Frederica Vitarelli[5], Claudio Caccia[6], Valerio Leoni[5], Bijan Ghaleh[1], Sandrine Pons[1] and Didier Morin[1]

Corresponding author: Didier MORIN, PhD, INSERM U955, Team Ghaleh, Faculté de Santé, 8 rue du général Sarrail, 94000, Créteil, France, E-mail : didier.morin@inserm.fr.

SUPPLEMENTARY METHODS

Synthesis of the cholesterol-resorufin probe

Cholesterol-resorufin probe (**F**) was prepared from 3β-acetoxy-22,23-bisnor-5-cholenic acid (**A**) according to a modified version of the procedure initially described (Simpson et al., 1991). This synthesis includes five steps as follows (following figure):

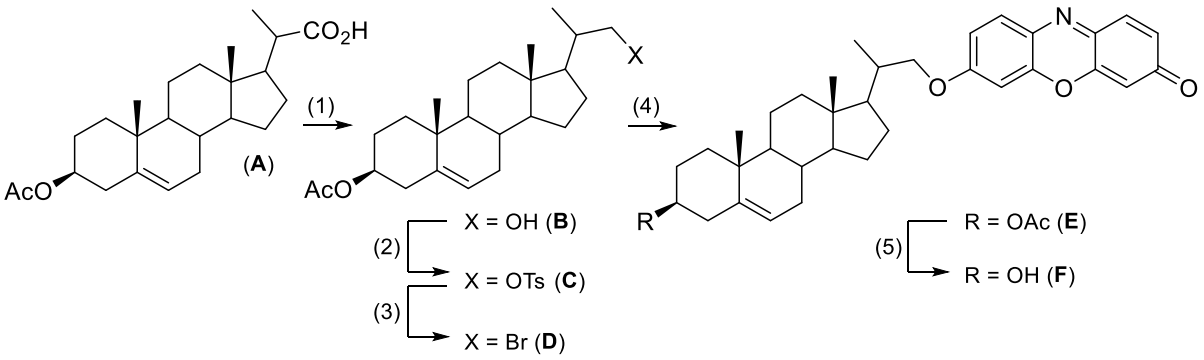

(1) (a) oxalyl chloride, RT, tetrahydrofuran; (b) $LiAlH(OtBu)_3$, -60 °C, tetrahydrofuran, quantitative.
(2) tosyl chloride, triethylamine, 4-(dimethylamino)pyridine, 50 °C, dichloromethane, 50%.
(3) LiBr, 60 °C, *N,N*-dimethylformamide, quantitative.
(4) resorufin, K_2CO_3, 50 °C, *N,N*-dimethylformamide, 65%.
(5) $LiAlH_4$, 0 °C, tetrahydrofuran, 45%.

(1) Preparation of alcohol (**B**): to a stirred solution of acid (**A**) (1 g, 2.57 mmol) in anhydrous dichloromethane, was added oxalyl chloride (1.5 equiv, 325 microL) dropwise at 0 °C. After 2 h at room temperature, the reaction mixture was concentrated under reduced pressure and the resulting solid dissolved in anhydrous tetrahydrofuran under argon. To this solution, lithium tri-t-butoxy aluminum hydride $(LiAlH(OtBu)_3$ (2.7 equivalent, prepared from lithium aluminium hydride ($LiAlH_4$, 624 mg, 7 mmol) and tert-butanol (1.54 g, 20.8 mmol) in tetrahydrofuran) was added dropwise and under stirring at -60 °C. The mixture was kept at -60 °C for 2.5 h. After dilution with diethyl ether, an aqueous solution of concentrated NaOH was added dropwise to precipitate the aluminum salts. After filtration over a celite pad, the organic phase was washed with HCl (1N), with brine and dried over $MgSO_4$. The NMR analysis confirmed the complete conversion of the acid (**A**) into the alcohol (**B**), which was used without further purification. Alcohol (**B**) was obtained as a white powder (950 mg, quantitative).

(2) Preparation of tosylate (**C**): to a stirred solution of (**B**) (893 mg, 2.38 mmol) in anhydrous dichloromethane were successively added 4-toluenesulfonyl chloride (2 equiv, 910 mg), triethylamine (4.2 equiv, 1.39 mL) and 4-(dimethylamino)pyridine (5%, 14 mg). The mixture was refluxed for 15 h, then successively diluted with

dichloromethane, washed with HCl (1 N), dried over $MgSO_4$ and concentrated under reduced pressure. After purification by chromatography on silica gel (cyclohexane/ethyl acetate, 90:10), the tosylate (**C**) was obtained as a white powder (629 mg, 50%).

(3) Preparation of brominated compound (**D**): to a stirred solution of (**C**) (629 mg, 1.19 mmol) in anhydrous *N*,*N*-dimethylformamide (3.2 mL) was added LiBr (3 equiv, 310 mg), and the resulting mixture was heated at 60 °C for 15 h. After dilution with H_2O, the aqueous phase was extracted with cyclohexane. Brominated compound (**D**) was obtained as a white powder (515 mg, quantitative).

(4) Preparation of ether (**E**): to a stirred solution of (**D**) (160 mg, 0.36 mmol) in anhydrous *N*,*N*-dimethylformamide (3 mL), were successively added resorufin (1.3 equiv, 101 mg) and K_2CO_3 (2 equivalents, 100 mg). The resulting mixture was heated at 50 °C for 6 days under Ar. After dilution with H_2O, the aqueous phase was extracted with dichloromethane. The combined organic layers were washed with K_2CO_3 and dried over $MgSO_4$. After purification by chromatography on silica gel (cyclohexane/ethyl acetate, 70:30), the ether (**E**) was obtained as an orange solid (135 mg, 65%).

(5) Preparation of cholesterol-resorufin probe (**F**): to a stirred solution of (**E**) (101 mg, 0.18 mmol) in anhydrous tetrahydrofuran at 0 °C, was added $LiAlH_4$ (1.5 equiv, 10 mg). The mixture was let to react for 15 min at 0 °C and hydrolyzed with HCl (1N). The mixture was extracted with dichloromethane and the organic layers were dried over $MgSO_4$ and concentrated under reduced pressure. After purification by chromatography on silica gel (cyclohexane/ethyl acetate/triethylamine, 80:20:1%), the probe (**F**) was obtained as a red solid (42 mg, 45%).

Evaluation of CYP11A1 activity

CYP11A1 activity was measured in rat ventricular and testicular mitochondrial fractions as the ketokonazole inhibitable resorufine release induced by the enzyme according to a modified procedure described previously (Rone at al., 2012). Mitochondria were broken by 3 successive freeze-thaw cycles and were incubated at two concentrations 0.5 and 1 mg/ml in a buffer including 250 mM sucrose, 10 mM phosphate buffer, 15 mM triethanolamine-HCl, 20 mM KCl, 5 mM $MgCl_2$, 5 µM trilostane (pH=7 at 30°C). The reaction was then initiated by the successive addition of 5 µM cholesterol-resorufin and 500 µM NADPH. CYP11A1 activity was monitored over time by monitoring the

release of resorufin, which was followed by measuring the increase in fluorescence using a fluorescence spectrometer (Jasco FP-6300, excitation wavelength 530 nm; emission wavelength 595 nm). Ketokonazole (20 M) was added to evaluate the release of resorufin specifically related to CYP11A1 activity.

Assessment of mitochondrial respiratory complex activities

Mitochondrial respiratory chain enzymatic activities were measured as previously reported but with some modifications (Zini et al., 2007; Lo Iacono et al., 2011). Briefly, mitochondrial complex I activity (NADH decylubiquinone oxidoreductase) was measured at 37°C by monitoring the decrease in absorbance resulting from the oxidation of NADH at 340nm. The incubation medium contained 25 mM KH_2PO_4, 5 mM $MgCl_2$, 100 µM NADH, 250 µM KCN, 1 mg/ml bovine serum albumin and 0.04 mg/ml of freeze-thawed heart mitochondria. The reaction was started by the addition of 100 µM decylubiquinone.

Mitochondrial complex II activity (succinate ubiquinone reductase) was measured by monitoring the absorbance changes of 2,6-dichloroindophenol at 600 nm. The assay mixture contained 10 mM KH_2PO_4, 2 mM EDTA, 2 µM rotenone, 6 mM succinate, 250 µM KCN, 1 mg/ml bovine serum albumin and 0.02 mg/ml of freeze-thawed heart mitochondria. After a preincubation period of 5 min at 37°C, and addition of 80 µM 2,6-dichloroindophenol, the reaction was initiated by the addition of 100 µM decylubiquinone.

Ubiquinol cytochrome c reductase activity (complex III) was measured at 37°C as the rate of cytochrome c reduction at 550 nm. The reaction mixture contained 10 mM KH_2PO_4, 2 mM EDTA, 2 µM rotenone, 250 µM KCN, 1 mg/ml bovine serum albumin, 40 µM oxidized cytochrome c, 0.01 mg/ml of freeze-thawed heart mitochondria. The reaction was started by the addition of 100 µM decylubiquinol.

Mitochondrial complex IV activity (cytochrome c oxidase) was performed at 550 nm following the decrease in absorbance resulting from the oxidation of reduced cytochrome c. The reaction mixture contained 10 mM KH_2PO_4, 2 mM EDTA, 2 mM $MgCl_2$, 33 µM oxidized cytochrome c and 0.01 mg/ml of freeze-thawed heart mitochondria. The reaction was started by the addition of 1 mM of lauryl maltoside. Complex activities were quantified by measuring the initial slopes of the absorbance curves.

Determination of cholesterol and oxysterol levels

Sterol and oxysterol measurements were performed on cytosolic and mitochondrial extracts. To a screw-capped vial sealed with a Teflon septum, mitochondrial or cytosolic samples were added together with 50 ng of D7-7α-hydroxycholesterol, D7-7β-hydroxycholesterol, D7-7ketocholesterol, D6-cholesterol-5α,6α-epoxide, D6-cholesterol-5β,6β-epoxide and D6-27-hydroxycholesterol as internal standards, 50 µl of butylated hydroxytoluene (5 g/L) and 50 µl of K3-EDTA (10 g/L) to prevent auto oxidation. Each vial was flushed with argon for 20 min to remove air. Alkaline hydrolysis was allowed to proceed at room temperature (22°C) with magnetic stirring for 30 minutes in the presence of ethanolic 1M potassium hydroxide solution. After hydrolysis, the sterols were extracted twice with 5 ml cyclohexane and oxysterols were eluted on SPE cartridge by isopropanol:hexane 30:70 v/v. The organic solvents were evaporated under a gentle stream of argon and converted into trimethylsilyl ethers with BSTFA.

Analysis was performed by gas chromatography – isotope dilution mass spectrometry (GC-MS) with a B-XLB column (30 m × 0.25 mm i.d. × 0.25 µm film thick-ness, J&W Scientific Alltech, Folsom, CA, USA.) in a HP 6890 Network GC system (Agilent Technologies, USA) connected with a direct capillary inlet system to a quadruple mass selective detector HP5975B inert MSD (Agilent Technologies, USA). GC system was equipped with a HP 7687 series autosamplers and HP 7683 series injectors (Agilent Technologies, USA). The oven temperature program was as follows: initial temperature of 180 °C was held for 1 min, followed by a linear ramp of 20 °C/min to 270 °C, and then a linear ramp of 5 °C/min to 290 °C, which was held for 10 min. Helium was used as carrier gas at a flow rate of 1 mL/min and 1 µL of sample was injected in splitless mode.

Injection was carried at 250 °C with a flow rate of 20 ml/min. Transfer line temperature was 290 °C. Filament temperature was set at 150 °C and quadrupole temperature at 220 °C according with the manufacturer indication. Mass spectrometric data were acquired in selected ion monitoring mode

(OTMSi-ethers) at m/z = 463 (M+-90) for 7β-hydroxycholesterol-d7, m/z = 456 (M+-90) for 7β-hydroxycholesterol, m/z = 479 (M+-90) for 7-ketocholesterol-d7, m/z = 472 (M+-90) for 7-ketocholesterol, m/z = 462 (M+-90) for 27-hydroxycholesterol-d6 and m/z = 456 (M+-90) for 27-hydroxycholesterol, m/z = 481 for 5α,6α-epoxycholestanol-d7, m/z = 474 for 5α,6α-epoxycholestanol, m/z = 481 for 5ß,6ß-epoxycholestanol-d7, m/Z 474 for 5ß,6ß-epoxycholestanol. Peak integration was performed manually, and oxysterols were quantified from selected-ion monitoring analysis against internal standards using standard curves for the listed sterols (Civra et al., 2019).

References

Simpson DJ, Unkefer CJ, Whaley TW, Marrone BL (1991) A Mechanism-Based Fluorogenic Probe for the Cytochrome P-450 Cholesterol Side Chain Cleavage Enzyme. J Org Chem 56:5391-5396 doi: 10.1210/endo-128-5-2654

Zini R, Berdeaux A, Morin D (2007) The differential effects of superoxide anion, hydrogen peroxide and hydroxyl radical on cardiac mitochondrial oxidative phosphorylation. Free Radic Res 41:1159-1166 doi: 10.1080/10715760701635074

Lo Iacono L, Boczkowski J, Zini R, Salouage I, Berdeaux A, Motterlini R, Morin D (2011) A carbon monoxide-releasing molecule (CORM-3) uncouples mitochondrial respiration and modulates the production of reactive oxygen species. Free Radic Biol Med 50:1556-1564 doi: 10.1016/j.freeradbiomed.2011.02.033

Rone MB, Midzak AS, Issop L, Rammouz G, Jagannathan S, Fan J, Ye X, Blonder J, Veenstra T, Papadopoulos V (2012) Identification of a dynamic mitochondrial protein complex driving cholesterol import, trafficking, and metabolism to steroid hormones. Mol Endocrinol 26:1868-1882 doi: 10.1210/me.2012-1159

Civra A, Leoni V, Caccia C, Sottemano S, Tonetto P, Coscia A, Peila C, Moro GE, Gaglioti P, Bertino E, Poli G, Lembo D (2019) Antiviral oxysterols are present in human milk at diverse stages of lactation. J Steroid Biochem Mol Biol 193:105424 doi: 10.1016/j.jsbmb.2019.105424

SUPPLEMENTARY FIGURES

Fig. S1

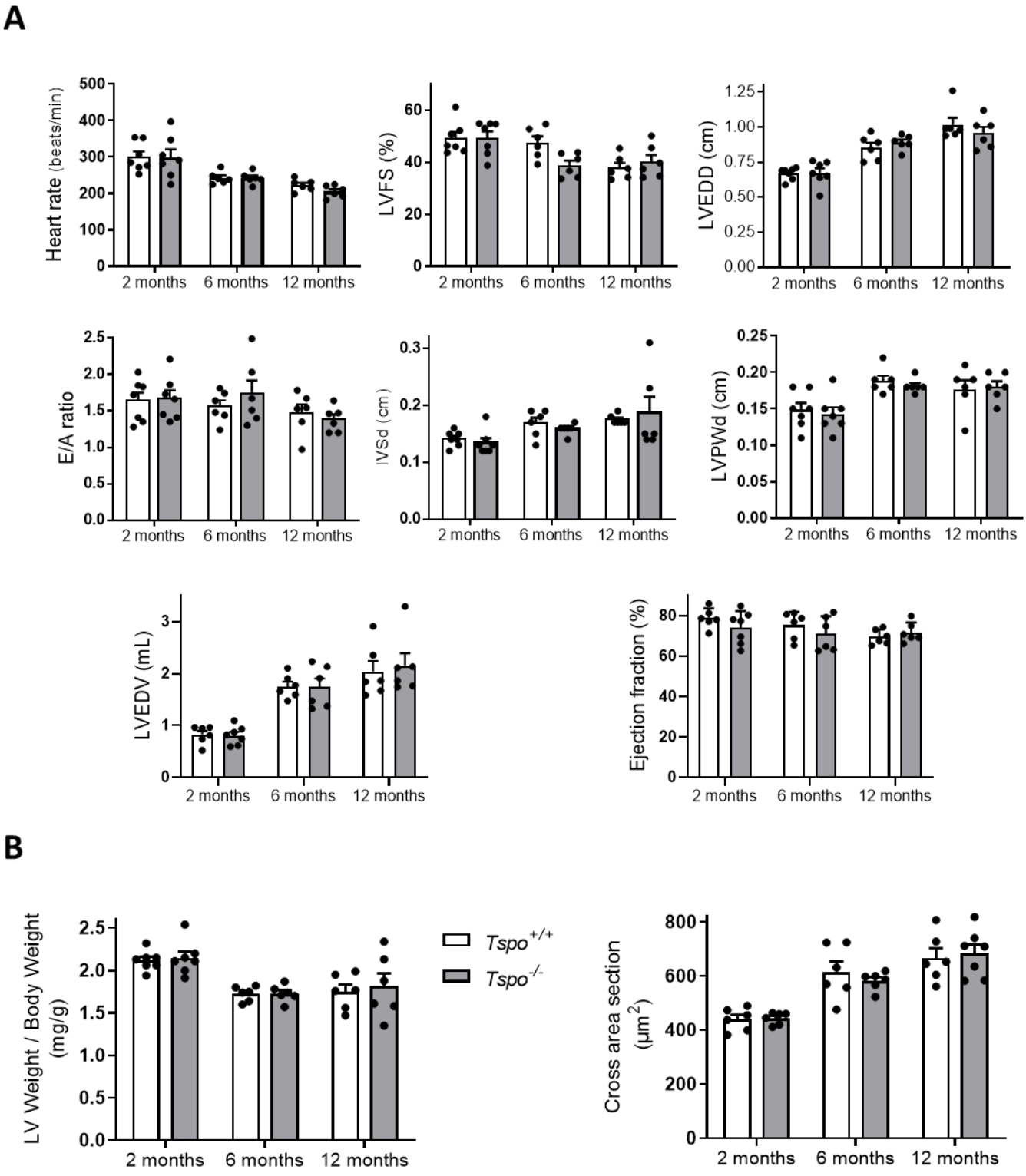

Fig. S1 TSPO deletion does not alter rat cardiac phenotype during aging.
Cardiac parameters were evaluated in 2-, 6- and 12-month-old rats.
A: Echocardiographic parameters: Left ventricular fractional shortening (LVFS), mitral E wave/A wave ratio (E/A ratio), left ventricular end-diastolic diameter (LVEDD), interventricular septum thickness in diastole (IVSd), Left Ventricular Posterior Wall thicknesses in Diastole (LVPWd), left ventricular end-diastolic volume (LVEDV). Each value is the mean ± SEM of at least 6 animals.
B: Indexes of ventricular hypertrophy in *Tspo*$^{+/+}$ and *Tspo*$^{-/-}$ rats.
Left: ventricular (LV) weight to body weight ratio. Each value is the mean ± SEM of at least 6 animals.
Right: cross sections of left ventricular were stained with FITC-conjugated WGA and cardiomyocyte surface in each section was quantified using Image J. Each value is the mean ± SEM of at least 6 animals, i.e., 1080 cells (6 ventricles, 6 sections by ventricle and 30 cells by section).
In all panels, statistical comparison between genotypes were done using a two-way ANOVA. No difference between genotypes was observed whatever the parameter.

Fig. S2

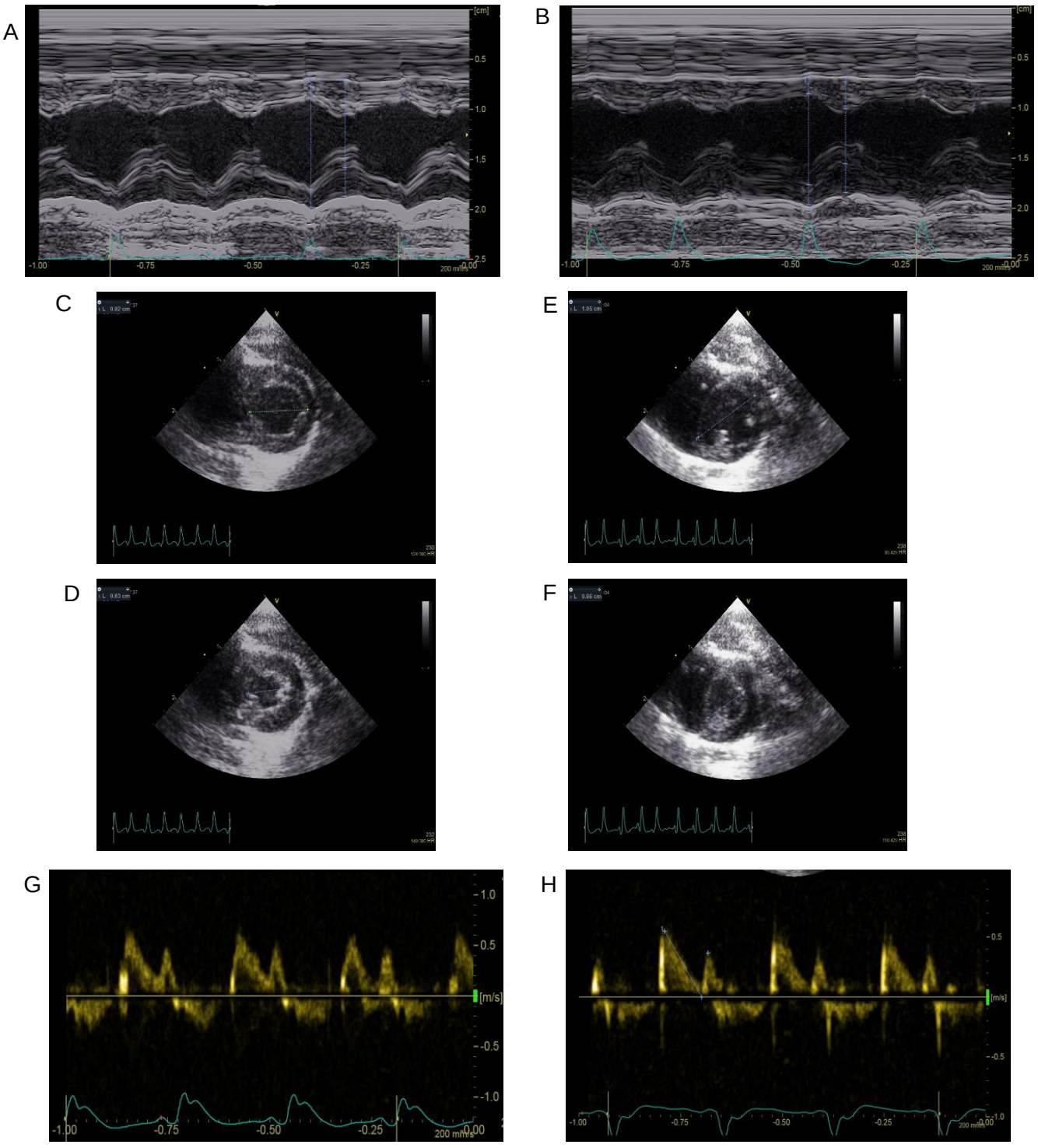

Fig. S2 Typical examples of analysis of LV dimensional parameters and LVFS from M-mode images obtained in one 6-month-old *Tspo*$^{+/+}$ (A) and one 6-month-old *Tspo*$^{-/-}$ rat (B).

Measurement of LV internal diameter in the end-diastole and end-systole from the cine loop of the parasternal short-axis view at the level of papillary muscles for the calculation of EF using Teicholz formula in one 6-month-old *Tspo*$^{+/+}$ rat (C, D) and one 6-month-old *Tspo*$^{-/-}$ rat (E, F), and measurement of E and A velocities and their ratio using transmitral flow tracing obtained by pulse wave *Doppler in* one 12-month-old *Tspo*$^{+/+}$ rat (G) and one 12-month-old *Tspo*$^{-/-}$ rat (H).

Fig. S3

A

Coupling	Pups / litter	Sexe		Genotype			litters
		Female	Male	*Tspo*$^{+/+}$	*Tspo*$^{+/-}$	*Tspo*$^{-/-}$	
Homozygote *Tspo*$^{+/+}$	11±1	60%	40%	100%	x	x	18
Homozygote *Tspo*$^{-/-}$	12±1	55%	45%	x	x	100%	22
Heterozygote *Tspo*$^{+/-}$	10±1	51%	49%	27%	47%	25%	19

B

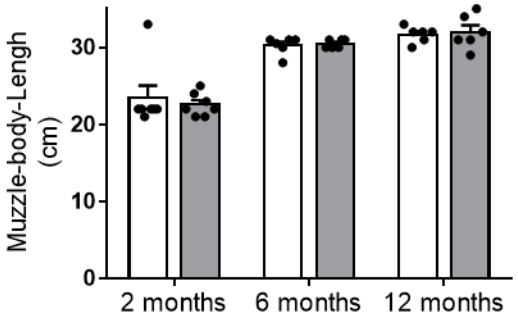

C

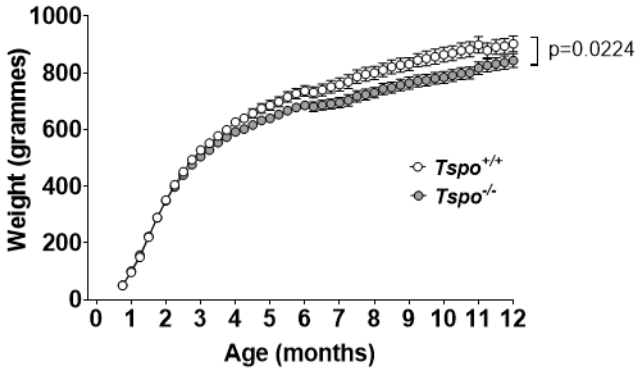

D

Steroid hormones (ng/ml)	2 months		6 months		12 months	
	Tspo$^{+/+}$	*Tspo*$^{-/-}$	*Tspo*$^{+/+}$	*Tspo*$^{-/-}$	*Tspo*$^{+/+}$	*Tspo*$^{-/-}$
Pregnenolone	0.26±0.02	0.28±0.02	0.51±0.05	0.59±0.05	1.16±0.12	1.21±0.13
Progesterone	0.180±0.009	0.177±0.006	0.210±0.005	0.212±0.004	0.55±0.03	0.52±0.02
Deoxycorticosterone	0.304±0.007	0.296±0.005	0.624±0.002	0.60±0.01	1.08±0.05	1.09±0.04
Corticosterone	98.4±2.70	98.8±1.59	130.0±3.81	133.3±2.75	146.6±2.44	142.9±3.68
Aldosterone	0.303±0.005	0.296±0.006	0.237±0.004	0.223±0.004	0.177±0.005	0.169±0.004
17OH-Progesterone	0.47±0.06	0.45±0.08	1.33±0.15	1.16±0.21	1.84±0.37	1.62±0.26
Cortisol	4.20±0.43	3.65±0.48	5.49±0.48	6.28±0.59	5.52±0.43	4.80±0.32
Dehydroepi-androsterone	0.55±0.07	0.54±0.11	0.56±0.05	0.62±0.04	0.88±0.08	0.76±0.06
D4-androstenedione	0.41±0.04	0.43±0.02	0.48±0.06	0.45±0.03	0.45±0.04	0.54±0.07
Testosterone	1.33±0.20	1.29±0.19	2.08±0.47	1.07±0.15	1.51±0.22	1.51±0.21
Dihydrotestosterone	0.043±0.016	0.026±0.008	0.068±0.020	0.025±0.006*	0.037±0.007	0.030±0.008
Oestradiol (x 10^{-3})	2.11±0.12	2.04±0.09	2.12±0.10	1.89±0.06	1.67±0.08	1.42±0.07
Androsterone	0.060±0.005	0.058±0.006	0.056±0.005	0.042±0.002	0.052±0.003	0.048±0.004

Fig. S3 Reproduction parameters (**A**) and evolution of body lengths (**B**), body weights (**C**) and circulating steroidogenic hormones (**D**) in *Tspo*$^{+/+}$ *and Tspo*$^{-/-}$ rats during aging. **B**: each value is the mean ± SEM of 6-7 animals. **D**: values are means ± SEM, n=8 (*Tspo*$^{+/+}$) and n= 10 rats (*Tspo*$^{-/-}$). Statistical comparison between genotypes in panel B and D were done by a two-way ANOVA analysis followed by a Sidak multi-comparison test. *p=0.0237 *vs* respective *Tspo*$^{+/+}$. Statistical analysis in panel **C** was done using a mixed effect analysis.

Fig. S4

A

Age	Glycemia mg/dL		Cholesterol mmol/L		HDL mmol/L		Triglycerides mmol/L		Free Fatty Acid mmol/L	
months	*Tspo*$^{+/+}$	*Tspo*$^{-/-}$	*Tspo*$^{+/+}$	*Tspo*$^{-/-}$	*Tspo*$^{+/+}$	*Tspo*$^{-/-}$	*Tspo*$^{+/+}$	*Tspo*$^{-/-}$	*Tspo*$^{+/+}$	*Tspo*$^{-/-}$
2	127 ± 4	119 ± 3	2.49 ± 0.08	2.52 ± 0.11	1.44 ± 0.06	1.36 ± 0.06	2.43 ± 0.24	2.13 ± 0.12	1.00 ± 0.06	0.93 ± 0.04
6	107 ± 3	99 ± 1	3.08 ± 0.15	3.22 ± 0.12	1.63 ± 0.09	1.72 ± 0.07	2.53 ± 0.23	2.64 ± 0.23	0.99 ± 0.06	1.00 ± 0.05
12	110 ± 2	105 ± 3	3.46 ± 0.16	3.44 ± 0.13	1.85 ± 0.09	1.92 ± 0.06	2.11 ± 0.21	1.81 ± 0.10	1.06 ± 0.05	1.00 ± 0.03

B

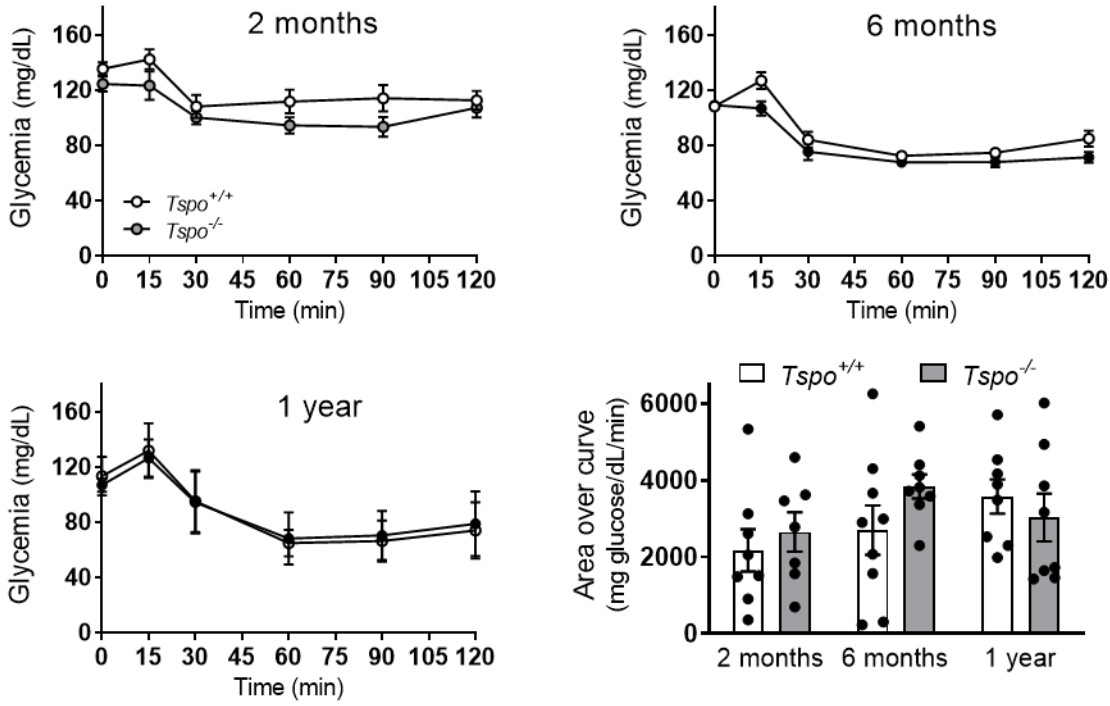

C

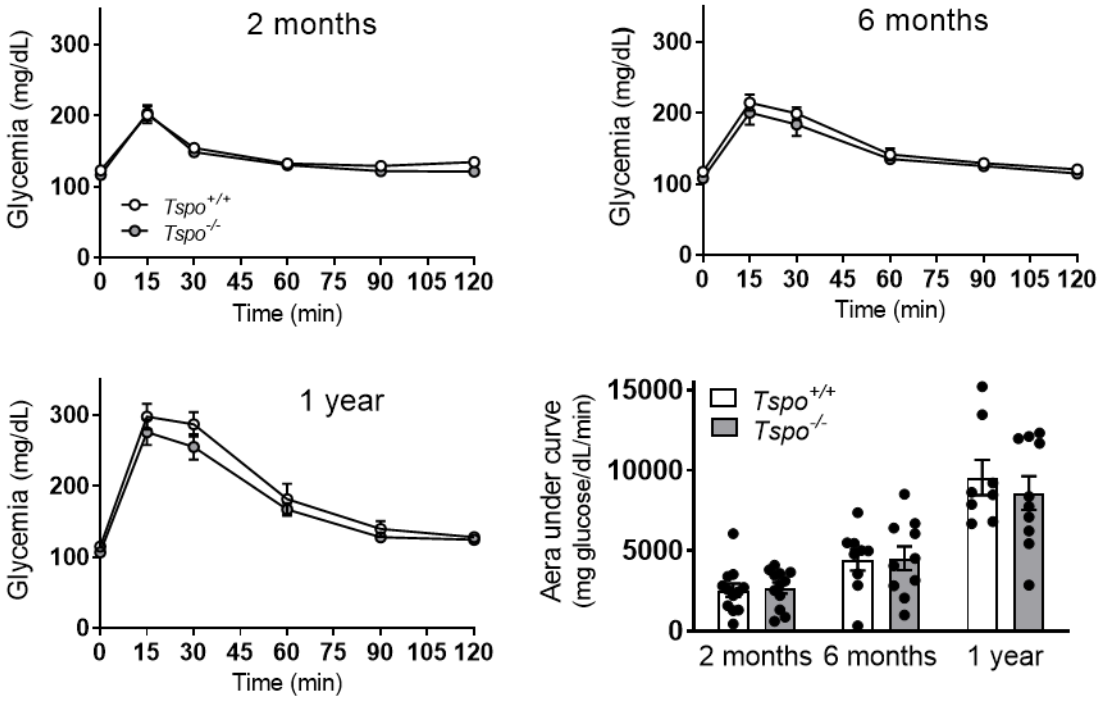

Fig. S4 Glycemia, lipid blood levels and effect of metabolic stresses in *Tspo*$^{+/+}$ and *Tspo*$^{-/-}$ rats during aging.

A: glycemia and lipid blood levels in 2-, 6- and 12-month-old rats. Each value is the mean ± SEM, n=7-10 animals.

B: Insulin tolerance tests performed in 2-, 6- and 12-month *Tspo*$^{+/+}$ and *Tspo*$^{-/-}$ rats. At t=0, fasting rats received 1 UI/kg insulin. Glycemia was measured for 2 hours and the areas over the curve (AOC) were calculated (bar graph). Each value is the mean ± SEM, n=7-9 animals.

C: Glucose tolerance tests performed in 2-, 6- and 12-month *Tspo*$^{+/+}$ and *Tspo*$^{-/-}$ rats. At t=0, fasting rats received 1 g/kg D-glucose. Glycemia was measured for 2 hours and the areas under the curve (AUC) were calculated (bar graph).

Each value is the mean ± SEM, n=8-12 animals. Statistical comparison between genotypes (**A** and bar graphs of **B** and **C**) were done by a two-way ANOVA analysis. No difference between genotypes was observed whatever the parameter.

Fig. S5

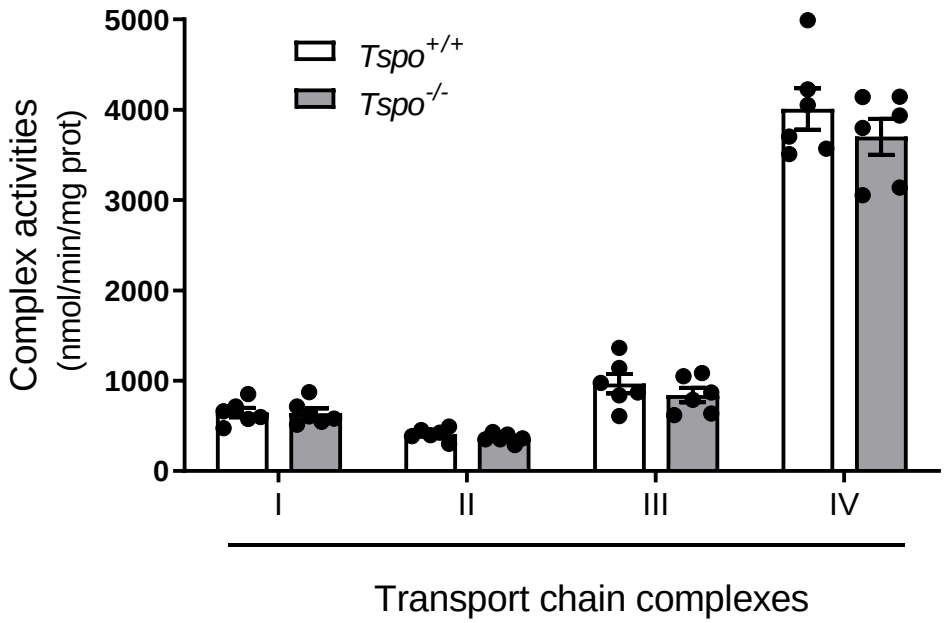

Fig. S5 Activities of transport chain complexes in *Tspo*$^{+/+}$ and *Tspo*$^{-/-}$ rats.
Enzymatic activities of each respiratory chain complex (nmol/min/mg protein) were measured in mitochondrial fractions prepared from hearts of *Tspo*$^{+/+}$ and *Tspo*$^{-/-}$ rats.
Each value is the mean ± SEM of 6 independent preparations (6 animals). Statistical comparison between genotypes was done by a using an unpaired two-tailed t-test. No difference between genotypes was observed whatever the complex.